

Modelling droplet collision outcomes for different substances and viscosities

Martin Sommerfeld¹ · Matthias Kuschel¹

Received: 3 February 2016 / Revised: 14 September 2016 / Accepted: 14 September 2016 / Published online: 19 November 2016
© Springer-Verlag Berlin Heidelberg 2016

Abstract The main objective of the present study is the derivation of models describing the outcome of binary droplet collisions for a wide range of dynamic viscosities in the well-known collision maps (i.e. normalised lateral droplet displacement at collision, called impact parameter, versus collision Weber number). Previous studies by Kuschel and Sommerfeld (Exp Fluids 54:1440, 2013) for different solution droplets having a range of solids contents and hence dynamic viscosities (here between 1 and 60 mPa s) revealed that the locations of the triple point (i.e. coincidence of bouncing, stretching separation and coalescence) and the critical Weber number (i.e. condition for the transition from coalescence to separation for head-on collisions) show a clear dependence on dynamic viscosity. In order to extend these findings also to pure liquids and to provide a broader data basis for modelling the viscosity effect, additional binary collision experiments were conducted for different alcohols (viscosity range 1.2–15.9 mPa s) and the FVA1 reference oil at different temperatures (viscosity range 3.0–28.2 mPa s). The droplet size for the series of alcohols was around 365 and 385 μm for the FVA1 reference oil, in each case with fixed diameter ratio at $\Delta = 1$. The relative velocity between the droplets was varied in the range 0.5–3.5 m/s, yielding maximum Weber numbers of around 180. Individual binary droplet collisions with defined conditions were generated by two droplet chains each produced by vibrating orifice droplet generators. For recording droplet

motion and the binary collision process with good spatial and temporal resolution high-speed shadow imaging was employed. The results for varied relative velocity and impact angle were assembled in impact parameter–Weber number maps. With increasing dynamic viscosity a characteristic displacement of the regimes for the different collision scenarios was also observed for pure liquids similar to that observed for solutions. This displacement could be described on a physical basis using the similarity number and structure parameter K which was obtained through flow process evaluation and optimal proportioning of momentum and energy by Naue and Bärwolff (Transportprozesse in Fluiden. Deutscher Verlag für Grundstoffindustrie GmbH, Leipzig 1992). Two correlations including the structure parameter K could be derived which describe the location of the triple point and the critical We number. All fluids considered, pure liquids and solutions, are very well fitted by these physically based correlations. The boundary model of Jiang et al. (J Fluid Mech 234:171–190, 1992) for distinguishing between coalescence and stretching separation could be adapted to go through the triple point by the two involved model parameters C_a and C_b , which were correlated with the relaxation velocity $u_{\text{relax}} = \sigma / \mu$. Based on the predicted critical Weber number, denoting the onset of reflexive separation, the model of Ashgriz and Poo (J Fluid Mech 221:183–204, 1990) was adapted accordingly. The proper performance of the new generalised models was validated based on the present and previous measurements for a wide range of dynamic viscosities (i.e. 1–60 mPa s) and liquid properties. Although the model for the lower boundary of bouncing (Estrade et al. in J Heat Fluid Flow 20:486–491, 1999) could be adapted through the shape factor, it was found not suitable for the entire range of Weber numbers and viscosities.

✉ Martin Sommerfeld
martin.sommerfeld@iw.uni-halle.de

¹ Mechanische Verfahrenstechnik, Zentrum für Ingenieurwissenschaften, Martin-Luther-Universität Halle-Wittenberg, 06099 Halle (Saale), Germany

List of symbols

B	Non-dimensional impact parameter (see Eq. 3)
b	Lateral displacement of the droplet centres upon collision (Fig. 2)
C_a, C_b	Parameter of Jiang et al. (1992) model, Eq. 18
Ca	Capillary number
d_1, d_S	Small droplet diameter
d_2, d_L	Large droplet diameter
f	Dimensionless property
f^*	Dimensionless effort function for the self-organising process
h	Parameter in Eq. 15
K	Structure parameter characterising the optimal proportioning of flow motion in mainstream direction and structure agitation
m_1, m_2, m_3	Masses of the droplets before (1, 2) and after collision (3)
Oh	Ohnesorge number
$P_{1,2}$	Directional vector of the centres of mass of colliding droplets
PTV	Particle tracking velocimetry
$phas_1, phas_2$	Average effect of the structure agitation caused by the phase shift between two oscillating quantities
Re	Reynolds number
S	Dimensionless entropy
s_0, s_t	Travel distance of a particle in the centre of a residence volume
u_{rel}	Relative velocity
u_{relax}	Relaxation velocity
u_{relax}^*	Critical relaxation velocity
V_0, V_t	Residence volume
v_j	Momentum velocity
We	Weber number
We_{crit}	Critical Weber number at $B = 0$
Δ	Diameter ratio
μ	Dynamic viscosity of the liquid
ϕ_S, ϕ_L	Parameter for small and large droplets in Eq. 14
η_S, η_L	Parameter in Eq. 16
ξ	Parameter in Eq. 17
ρ	Density of the liquid
σ	Surface tension of the liquid
σ_*	Entropy production
τ	Parameter in Eqs. 15 and 20
σ_{i^*}	Information entropy
φ	Enclosed angle between the directional vector of the centres of mass and relative velocity vector (Fig. 2)

χ	Parameter in Eq. 19
ψ	Shape factor of the model of Estrade et al. (1999), Eq. 19

1 Introduction

Spraying processes are frequently found in a number of technical and industrial processes. Particularly, spray drying of solutions or suspensions for creating solid particles with certain desired properties, like porosity or solubility, has an immense importance. Relevant areas of application are pharmaceutical industry, food production, detergent production and agriculture, to name only a few. Here, the liquid is mostly pressed by high pressure through a small nozzle, resulting in atomisation and spray cone formation. The atomisation process with subsequently droplet break-up near the nozzle exit yields a broad droplet size distribution as well as a strong correlation between droplet size and their velocity. Most important in a spray dryer is the evaporation of the solvent from the droplets through the injected hot air stream. This process of solids formation is strongly governed by the temperature and velocity history experienced by the droplets. Consequently, evaporation yields an increase of solids content and hence viscosity; however, also surface tension and droplet density are modified (Blei and Sommerfeld 2007). As a result of the droplet size distribution naturally droplet's response to fluid flow and turbulence is different and therefore they will experience different velocity and temperature histories. Both phenomena affect the residence time of droplets/particles and eventually their drying state, as well as morphology at the dryer outlet. A very wide droplet size distribution and turbulence effects favour collisions between droplets, due to their different ability to follow flow structures. Hence, droplet collisions not only occur in the dense spray region close to the nozzle (Hou and Schmidt 2006) but also in recirculation regions of a spray dryer.

Consequently, the droplets and particles residing in a spray dryer are very heterogeneous with different sizes, velocities, temperatures and species properties (i.e. drying state, viscosity, surface tension and density). Therefore, there is a huge demand in extending droplet collision models for allowing the consideration of these different droplet properties. The present study focusses on the influence of dynamic viscosity on the droplet collision outcome and a generalisation of collision models in this respect.

Another important technical process where liquids with higher viscosities are used is spray combustion, especially in connection with the increasing consumption of biofuels which can have very different viscosities (see, e.g., de O

Macedo et al. 2013). Moreover, during the spray injection and combustion cycle the produced droplets experience pressure and temperature changes, yielding variations in dynamic viscosity. Therefore, also droplets with different and elevated viscosity may collide. A very important technological spray process is also the atomisation of metallic, ceramic or mineral melts for producing pure or composite powders. Such hot melts have also elevated dynamic viscosities depending on atomisation temperature. During solidification of the melt droplets, naturally viscosity is rising which affects droplet collision results within the spray. For producing composite powders from different melts (mostly having different viscosity) requires the use of two interacting spray nozzles in order to yield high collision rates (Fritsching and Gao 2010). Hence, colliding droplets generally have elevated viscosity, different size and frequently also different viscosity. Consequently, there is a huge demand in understanding and modelling the effect of viscosity on binary droplet collisions.

There are several possible collision outcomes, namely bouncing, coalescence and separation (Ashgriz and Poo 1990), which additionally will modify the droplet size spectrum. Naturally, coalescence will produce larger droplets whereas separation yields several smaller satellite droplets depending mainly on Weber number (Brenn et al. 2001; Ko and Ryou 2005). Such small droplets or particles are normally unwanted in spray drying and are eventually collected in the particle separators (e.g. cyclone or bag filter) mounted downstream of the air exit pipe of the spray dryer. If it would be possible to control the collision-induced separation of droplets by adjusting the flow conditions inside the dryer one could probably reduce the production of such fine powders. Another objective of spray drying is the on-purpose formation of agglomerated powders with certain morphology. This may be accomplished by installing several closely spaced spray nozzles at the roof of the dryer. Therefore, the sprays from the nozzles will interact, promoting collisions between droplets, and if the drying process has advanced enough, agglomerates will be formed from sticky primary particles. Similarly, the often applied fine particles return yields collisions between droplets and dry particles also affecting the resulting powder properties. Therefore, it is clear that droplet collisions in spray dryers are very important and there is a large need for understanding and modelling the collision outcome at higher liquid viscosities.

During the last two decades numerous experiments on droplet collisions were conducted with water (Ashgriz and Poo 1990), alkane series (Jiang et al. 1992; Qian and Law 1997), ethanol (Estrade et al. 1999), silicone oils (Willis and Orme 2003), diesel droplets (Chen 2007) and only a few with two different liquids (Gao et al. 2005; Chen 2007; Tsuru et al. 2010; Plancette et al. 2012). The common approach for characterising the collision outcome is based on using reduced two-dimensional collision maps (see Fig. 1), where the

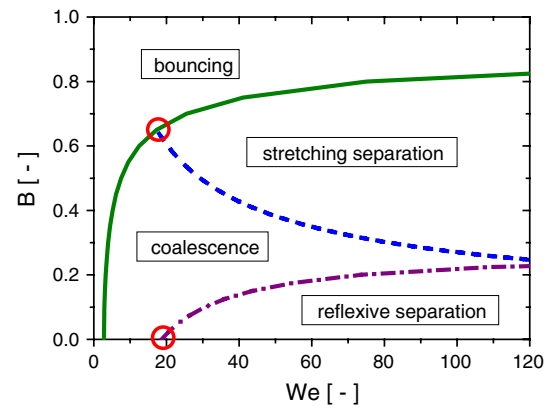


Fig. 1 Sketch of the commonly used collision map including the boundary lines between the different collision scenarios; circles (red) indicate the location of the triple point (*upper circle*) and the critical Weber number (*lower circle*)

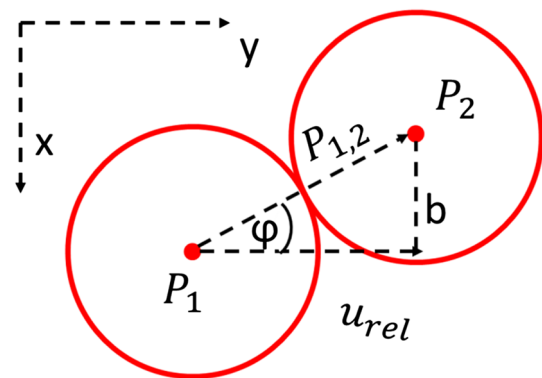


Fig. 2 Droplet collision geometry

normalised impact parameter is plotted versus the collision Weber number $B = f(We)$. The impact parameter results from the lateral displacement of colliding droplets (see Fig. 2), and the Weber number, which is the ratio of inertial force to the surface tension force, is given in Eq. 2. Hence, each experimental point may be marked in this map indicated with the collision outcome observed. It was found in many studies that in such collision maps the different collision outcomes may be clearly separated by boundary lines (see Appendix 1). However, these collision maps do not include all relevant droplet liquid and kinematic parameters of the collision process (see Eqs. 1–4) and therefore cannot be expected to be generally applicable. For example, the decrease in the droplet size ratio resulted in an upward shift of the boundary line between stretching separation and coalescence (Ashgriz and Poo 1990).

In most of the experimental studies mentioned above dynamic viscosities between 1 and 10 mPa s were considered. Jiang et al. (1992) recognised that different alkanes with increasing viscosity (in the range from 0.4 to 3.5 mPa s) show a shift of the onset of reflexive separation towards higher We numbers.

For silicon-based oils (viscosity 10 and 30 mPa s) Willis and Orme (2003) concentrated their work on the occurrence of head-on collisions, wherefore no information is available on the other collision scenarios. The main interest of this study was, however, the degree of unified droplet deformation during the head-on collision.

In the studies of Ashgriz and Poo (1990) the collision of water droplets and the involved deformation processes were experimentally studied in great detail for different collision scenarios up to $We = 100$. Surprisingly, however, no bouncing region was reported in this study. The main emphasis was to compare results for different droplet size ratios, namely $\Delta = 0.5, 0.75$ and 1.0 . When reducing the droplet size ratio also a shift of the separation regimes (i.e. reflexive and stretching separation) to higher Weber numbers was observed, as well as an upward shift of stretching separation and a downward shifting of reflexive separation.

Through the experiments of Jiang et al. (1992) the boundary lines for the region of coalescence were evaluated for different normal alkanes having dynamic viscosities between 0.4 and 3.5 mPa s. Therefrom, however, the extent of the region of stretching separation at higher Weber numbers cannot be identified.

The influence of ambient pressure and type of ambient gas on the collision of water and tetradecane droplets was investigated by Qian and Law (1997) presenting complete collision maps up to $We = 50$ and 100 , respectively. For water droplets in nitrogen gas at ambient pressure also the occurrence of bouncing was reported. With rising pressure (i.e. up to 8 bar) the region of bouncing increased dramatically associated with a shift of the occurrence of stretching separation to higher We . It was also shown that the type of ambient gas has a remarkable effect on the collision maps.

Binary collisions of ethanol droplets were investigated by Estrade et al. (1999) for the droplet size ratios of $\Delta = 1.0$ and $\Delta = 0.5$ and for Weber numbers up to 220 and 150, respectively. Their developed correlation for the lower boundary of bouncing based on an energy balance fitted the experimental results for both size ratios reasonably well (see Appendix 1). Between coalescence and stretching separation the correlation proposed by Brazier-Smith et al. (1972) was modified, and for the beginning of reflexive separation a corrected version of the Ashgriz and Poo (1990) correlation was used. Reasonable agreement with the measurements is obtained for both boundaries and both size ratios. For separation also the number of observed satellite droplets was obtained.

More recently, Rabe and Malet (2010) experimentally studied the collision of water droplets with different size ratio (i.e. 0.5, 0.75 and 1.0). They also observed the upward movement of the region of stretching separation as well as the downward shift of reflexive separation region with decreasing size ratio. Also in this study no region of

bouncing was reported. Note, however, that another study of the same group (Foissac et al. 2010) clearly showed a bouncing region for colliding water droplets of the same diameter. This might be caused by a droplet size effect; Rabe and Malet (2010) used 450- μ m droplets, whereas Foissac et al. (2010) performed measurements with 300- μ m droplets. Interestingly however, Rabe and Malet (2010) found a way to generalise the collision maps with regard to droplet size ratio by using a symmetric Weber number which is the ratio of the kinetic energy of both droplets to the surface energy of both droplets. Using this non-dimensional number as the abscissa, instead of the standard Weber number, the regions of collision outcome for all three size ratios completely collapsed.

In the experimental studies of Gotaas et al. (2007b), different species (i.e. MEG, DEG, TEG, which are mono-, di- and triglycol) with viscosities between 22 and 48 mPa s were investigated and compared to results with theoretical boundaries between coalescence and stretching separation proposed by Ashgriz and Poo (2001) and Jiang et al. (1992). Only the latter model, which is based on a momentum balance and includes viscous dissipation, was able to describe the upward shift of this boundary with increasing viscosity. However, the occurrence of bouncing collisions was not investigated. Moreover, Gotaas et al. (2007b) established two matched correlations for the shift of the critical Weber number describing the beginning of reflexive separation at $B = 0$ with increasing dynamic viscosity.

Recently, Kuschel and Sommerfeld (2013) experimentally investigated the collision outcome for high viscous solution droplets (i.e. polyvinylpyrrolidone, PVP K17 and PVP K30 as well as sucrose) and complete collision maps were presented for Weber numbers up to about 100. Here the solids content was increased for each substance yielding also a modification of the relevant fluid properties (i.e. surface tension and liquid density) and especially a remarkable increase of the dynamic viscosity. It was clearly shown that viscosity has a strong influence on the extent and size of the regions for the different collision outcomes in the collision maps and also the beginning of separation (i.e. reflexive and stretching). An upward shift of the boundary between coalescence and stretching separation towards higher impact parameters was observed with increasing viscosity, similar as by Gotaas et al. (2007b). Consequently, the location of the “triple point” (collapse of bouncing, coalescence and stretching separation, see Fig. 1) is continuously changing with increasing viscosity and shows clearly extreme values with respect to relative velocity and impact parameter. The location of the maximum/minimum was identified to be at a Capillary number of about $Ca = 0.577$ for all the substances considered in this study (Kuschel and Sommerfeld 2013). Moreover, it was revealed that the onset of reflexive separation is shifted to higher

Weber numbers with increasing viscosity which has already been found by Jiang et al. (1992). Finally, also the number of satellite droplets produced by separative collisions was determined for all the substances. Two models for the boundary line between coalescence and stretching separation were considered (Kuschel and Sommerfeld 2013), but only the momentum balance model of Jiang et al. (1992) could be adapted through the variation of the involved two model parameters. It should be, however, emphasised that all available models lack a limiting point (here called triple point), at which separation ends and either coalescence or bouncing occurs, with the result that for lower Weber numbers the prediction by such a boundary line is meaningless.

As a conclusion from all the studies described above, it can be stated that the droplet collision maps are not universal but depend on numerous parameters, such as droplet properties and ambient gas conditions (i.e. droplet substance, droplet size and size ratio Δ , type of gas, gas pressure and temperature).

The present study is a continuation of the work done by Kuschel and Sommerfeld (2013) where the collision of solution droplets with a range of viscosities (i.e. between 1 and 60 mPa s) was studied. The objective of the present study relates to the generalisation of models with respect to the properties of droplet liquids, type of liquid and primarily the viscosity, for the boundaries between coalescence and stretching separation, coalescence and reflexive separation as well as the lower boundary of bouncing (Sommerfeld and Kuschel 2013). This model generalisation is based on the location and shift of the triple point (coincidence of bouncing, coalescence and stretching separation) and the critical We number for the beginning of reflexive separation at an impact parameter of zero as illustrated in Fig. 1. Unfortunately, most of the studies conducted so far for pure liquids do not provide information on the full collision map and hence these characteristic points. Therefore, additional experimental studies for pure liquids with different dynamic viscosity, namely for a series of alcohols and reference oil (FVA1) at different temperature, were conducted in order to complete the database. These data and those presented previously for solution droplets (Kuschel and Sommerfeld 2013) will be eventually used for deriving new generalised droplet collision models on a physical basis by accounting for viscosity effects employing the structure parameter K . The proposed new boundary lines are based on the momentum balance model of Jiang et al. (1992) for coalescence/stretching separation, the energy balance model of Ashgriz and Poo (1990) for coalescence/reflexive separation and the energy balance model of Estrade et al. (1999) for the lower bouncing boundary. The novel composite model is finally validated based on experiments for pure liquids and solutions with different dynamic viscosities.

2 Definition of relevant parameters

Collision outcomes of droplets are generally summarised in collision maps where the non-dimensional impact parameter B (Eq. 3) is plotted versus We (Eq. 2). By definition the non-dimensional impact parameter is the sinus of the enclosed angle φ between the relative velocity vector u_{rel} and the position vector $P_{1,2}$ between the droplets centre points (see Fig. 2).

The definitions of the relevant non-dimensional parameters to describe binary collisions of liquid droplets with identical liquids (implying identical viscosity, surface tension and density, so that the associated ratios do not appear in the set of parameters given below) as well as to create the collision maps and other diagrams presented in this paper are given below. The basic non-dimensional numbers are the Ohnesorge number Oh , only accounting for droplet size and substance properties, the collision Weber number We , the non-dimensional impact parameter B and droplet size ratio Δ :

$$Oh = \frac{\mu}{\sqrt{\rho \sigma d_1}} \quad (1)$$

$$We = \frac{\rho d_1 u_{rel}^2}{\sigma} \quad (2)$$

$$B = \frac{2b}{d_1 + d_2} = \sin \varphi \quad (3)$$

$$\Delta = \frac{d_1}{d_2} \quad (4)$$

Therefrom derived non-dimensional parameters are the Capillary number Ca and the Reynolds number Re .

$$Ca = \sqrt{We} Oh = \frac{\mu}{\sigma} u_{rel} = \frac{u_{rel}}{u_{relax}} \quad (5)$$

$$Re = \frac{\sqrt{We}}{Oh} = \frac{\rho d_1 u_{rel}}{\mu} \quad (6)$$

where d_1 and d_2 are the diameters of the small and large droplet, ρ , μ and σ are the density, dynamic viscosity and surface tension of the liquid, b is the lateral displacement of the droplet centres upon collision and φ the associated angle between relative velocity and the vector connecting the centres (Fig. 2), u_{rel} the relative velocity and $u_{relax} = \sigma/\mu$ the relaxation velocity; the latter results from the momentum conservation for plastic collisions. It should be mentioned that in the present study colliding droplets carry the same liquids and have identical sizes (i.e. $\Delta = 1$). Moreover, all experiments were conducted in the same ambient medium, namely at ambient pressure and normal room temperature.

3 Lagrangian droplet collision model

The present contribution is related to collisions of higher viscosity droplets and their outcomes as well as the modelling of droplet collisions in Lagrangian tracking approaches. The collision modelling for spray simulations involves the following steps:

- Detection of a possible collision between droplet pairs in a spray using either a deterministic model (O'Rourke 1981; note this model is based on calculating collision probabilities of any pair of parcels in a computational cell) or a stochastic approach (Rüger et al. 2000).
- For the stochastic collision model considered here, it is necessary to randomly sample the size and velocity of the fictitious collision partner being a representative of the local droplet population (Sommerfeld 2001) and other properties such as temperature and for solution droplets also the solids content. With that it is possible to obtain the droplet fluid properties such as material density, kinematic viscosity and surface tension.
- Consideration of impact probability which is relevant for a collision between a small and large droplet (Ho and Sommerfeld 2002), whereby the smaller droplet might move around the larger one with the relative velocity.
- Determination of instantaneous relative velocity (Sommerfeld 2001), collision Weber number and collision angle or impact parameter. When sampling the instantaneous velocity of the fictitious particle it is necessary to respect the correlation of the velocity of colliding droplets through fluid turbulence (Sommerfeld 2001).
- Using the well-known collision maps, where the impact parameter is plotted over collision Weber number, the type of collision is identified (i.e. bouncing, coalescence or stretching and reflexive separation). This, however, requires appropriate boundary lines between the different collision scenarios which are valid for the considered droplet fluids (see Fig. 1).
- The outcome of the droplet collision has to be determined for the collision type at hand based on mass and momentum balances (i.e. number of droplets, droplet sizes and their new velocities).

As mentioned above, the collision maps (i.e. $B = f(We)$) are not universal. Therefore, a proper modelling of droplet collisions would require experimental information for the desired droplet substances and conditions, which surely is very cumbersome if all relevant parameters are varied. A step-by-step generalisation of droplet collision models could resolve this problem to a large extent.

The boundary lines between different collision regimes were mainly derived on the basis of energy balances, comparing kinetic energies with the relevant surface energies. The models relevant to the present study are summarised in Appendix 1. The most commonly used approach for distinguishing between stretching separation and coalescence for water droplets was proposed by Brazier-Smith et al. (1972) defining a coalescence efficiency. Based on a more elaborated theory Ashgriz and Poo (1990) proposed also a boundary line stretching separation/coalescence (Fig. 1) again based on experiments for water, however considering also different droplet size ratios (see Appendix 1). A comparison of the proposed correlation with that of Brazier-Smith et al. (1972) showed good agreement for droplet size ratios around one. Larger differences were found especially for smaller Weber numbers and for droplet size ratios around 0.5. The Ashgriz and Poo (1990) model was also considered by Kuschel and Sommerfeld (2013), and it was found that it is not suitable for higher viscosities.

Jiang et al. (1992) studied the collision of water droplets as well as various hydrocarbon droplets which have a dynamic viscosity range between 0.4 and 3.5 mPa s. They found that the collision maps for hydrocarbons considerably deviate from that known for water since the different boundary lines are shifted to the right (i.e. to higher Weber numbers) when increasing the number of carbon atoms in the molecules. In order to capture dissipation effects, Jiang et al. (1992) derive the boundary between stretching separating and coalescence based on a momentum balance (see Appendix 1). The two involved model constants may be adapted according to the substance of the colliding droplets. Actually, this model was used by Gotaas et al. (2007a) and they successfully adapt the boundary line stretching separating/coalescence for different glycols with dynamic viscosities between 20 and 50 mPa s.

Finally, it should be emphasised that all the models for the boundary between stretching separation and coalescence do not predict a lower limit of validity, i.e. the location of the triple point.

For deriving the boundary between reflexive separation and coalescence (Fig. 1) Ashgriz and Poo (1990) proposed that the effective reflexive kinetic energy should be larger than 75% of the nominal surface energy of the combined spherical masses. The resulting correlation (see Appendix 1), however, only depends on the impact parameter and the droplet size ratio; viscosity is not accounted for.

Based on experimental studies for ethanol droplet collisions with different size ratio the lower boundary of bouncing (Fig. 1) was derived by Estrade et al. (1999) by the condition that the initial kinetic energy of droplet deformation should be smaller than the energy required to produce a limited deformation. Again the resulting correlation is dependent only on size ratio and impact parameter;

viscosity effects are neglected (see Appendix 1). Moreover, Estrade et al. (1999) adapted the stretching separation/coalescence boundary from Brazier-Smith et al. (1972) to fit their data for ethanol droplets.

Quite often, spray computations based on the Euler/Lagrange approach are done by only distinguishing between coalescence and grazing collision and neglecting all other possible collision outcomes (e.g. Gavaises et al. 1996; Rüger et al. 2000; Guo et al. 2004; Nijdam et al. 2006). Actually, this boundary line goes back to the work of O'Rourke (1981) which was termed coalescence efficiency in this work and specifies the critical impact parameter below which coalescence occurs. The associated correlation was derived based on the measurements of Brazier-Smith et al. (1972). In these single-boundary-line models only coalescence and grazing are considered as an outcome, where grazing implies that the two droplets continue their direction of motion after collision, but with reduced velocity magnitude due to dissipation (O'Rourke 1981). All other collision outcomes (e.g. reflexive separation or shattering) are neglected including also satellite formation. Especially in sprays where just downstream of the atomisation region the initial droplet concentration is quite high, droplet collisions will occur and influence the resulting droplet size distribution further downstream (Rüger et al. 2000). As a result, droplet coalescence yields an increase of the Sauter mean diameter along the spray, when averaged over the entire spray cross section (Rüger et al. 2000; Guo et al. 2004).

In the numerical computations of Post and Abraham (2002) for diesel spray injection the collision outcome was described by considering all collision scenarios. Hence, a hybrid model was used combining the boundary models of Estrade et al. (1999) for defining the lower boundary of bouncing, the Brazier-Smith et al. (1972) model for specifying the coalescence efficiency (i.e. upper boundary of coalescence) and the Ashgriz and Poo (1990) model to define the region of reflexive separation. Formation of smaller satellite droplets was only considered to occur due to shattering collision (Post and Abraham 2002). It was shown that when solely applying the Brazier-Smith et al. (1972) model the Sauter mean diameter along the spray increases at much higher rate compared to the proposed composite model. Consequently, collision maps and boundary lines obtained for "water" (note that only the Estrade et al. (1999) boundary line is obtained for Ethanol) are being used for the calculation of a diesel sprays. As illustrated in Fig. 10 of Post and Abraham (2002) all the boundary lines obtained for the model fuel Tetradecane (Qian and Law 1997) are shifted to higher We numbers, hence, it is not expected that the spray is predicted correctly with such an approach (Post and Abraham 2002). A comparison with measurements was, however, not performed. In

the composite droplet collision model used by Kollar et al. (2005) the same collision outcomes and the same boundary lines were considered, again neglecting satellite formation after separation.

A model for the appearance of satellite droplets after a separating collision was developed by Ko and Ryou (2005) in the frame of Euler/Lagrange calculations of two interacting sprays. The simulations showed that due to satellite droplet formation the Sauter mean diameter in the region of interacting sprays considerably decreases. Finally, also Munnannur and Reitz (2007) introduced a composite model for droplet collisions using the boundary lines for bouncing (Estrade et al. 1999), coalescence/stretching separation (Brazier-Smith et al. 1972) and reflexive separation (Ashgriz and Poo 1990). In the model for satellite droplet formation, they, however, include viscous dissipation, which was neglected by Ko and Ryou (2005). The comparison of the calculations with the proposed collision model showed a much better, though not perfect, agreement with measurements compared to neglecting satellite droplet formation. This brief summary confirms the need for more refined (possibly generalised) models describing the outcome of droplet collisions, especially by considering different liquid properties.

4 Experimental set-up

The experiments for analysing binary droplet collisions were carried out using two vibrating orifice droplet generators (producer: EncapBioSystems Inc., Greifensee, Switzerland, model number IE-0010H-P). The liquid was supplied by a pressurised storage vessel (Fig. 3). Mono-sized droplet chains were created by means of an excitation of the liquid being pressed through orifices with a diameter of 200 μm . The excitation frequency was for all liquids considered in the range between about 3600 and 4500 Hz which insured stable and regular break-up of the jet for the considered viscosity range. The resulting droplets were about 380 μm with a spacing of generally about 3 droplet diameters. For the considered droplet sizes and a nozzle exit velocity of about 5.1 m/s the droplet Reynolds number follows with $Re = 120$. Under this condition, the droplet wake is still symmetric and has a stream-wise extension of about one droplet diameter. As a consequence, the motion of the following droplets is barely disturbed which supports of course the stability of the droplet chain. Since the droplet chains were rather stable, the produced droplets had identical size and velocities, coalescence was rarely observed. In the present study only identical droplet sizes were considered, yielding a droplet diameter ratio $\Delta = 1$. Moreover, only collisions of droplets with identical liquid properties (i.e. viscosity and surface tension) are considered here. A

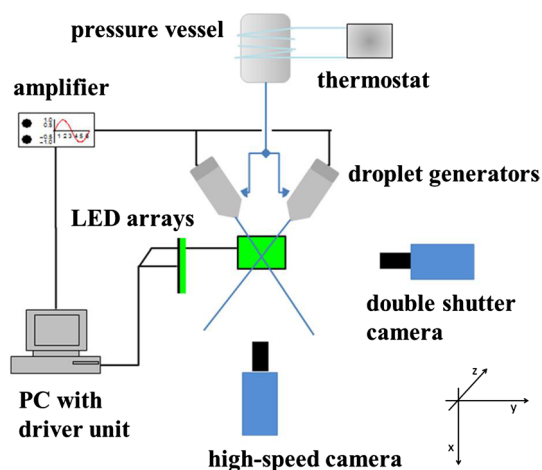


Fig. 3 Sketch of the experimental set-up with vibrating orifice droplet generators, imaging system with LED background illumination, recording cameras and controlling PC

thermostat was used in order to keep the liquid at a defined temperature.

The imaging of the droplet collision event and its outcome was based on background illumination by two LED arrays providing a uniform grey-level distribution in the region of interest. Two CCD cameras were used for recording shadow images of colliding droplets and produced liquid fragments. One high-speed camera (PCO 1200 HS) and one double-shutter camera (PCO sensicam Qe) were positioned perpendicular to each other. The high-speed camera recorded the collision event and the collision outcome in a front view, i.e. perpendicular to the collision plane. The double-shutter camera observed the collisions from the side, parallel to the collision plane. By this set-up any off-centre collisions could be detected and corrected to a large extent, so that position errors are below 3% (compare Kuschel and Sommerfeld (2013) for error estimation). The double-shutter camera operated at 5 frames per second (fps), whereas the high-speed camera recorded with 6000 fps to have an appropriate temporal resolution of the collision event. A suitable spatial resolution was achieved using Vicotar lenses (T100/0.48L) whereby the droplet diameter was resolved with around 16 pixels (i.e. $24.39 \mu\text{m}/\text{pixel}$). The images recorded by both cameras were stored on a PC for later processing. In order to obtain a sufficient dimension of the recorded imaging domain, in this case 1280×102 pixels, the resolution has to be limited to the value of $24.39 \mu\text{m}/\text{pixel}$. This implies that droplets smaller than this value cannot be resolved, which, however, was found to be sufficient as in the present study the size of the produced satellite droplets was not the main focus, although it could be estimated rather accurate in most cases. A series of images for a stretching separation

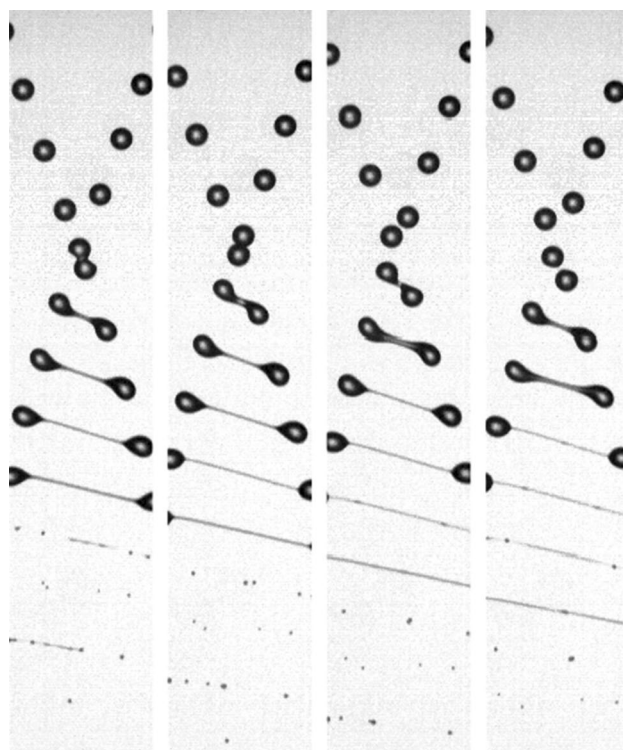


Fig. 4 Series of 4 collision images separated by $161 \mu\text{s}$ showing stretching separation of FVA1 oil droplets at a temperature of 23° , dynamic viscosity 28.2 mPa s , droplet diameter $385 \mu\text{m}$, $Oh = 0.282$, angle between droplet chains 39° , collision We number 75

where rather small satellites are produced is shown in Fig. 4, i.e. higher-viscous oil FVA1 at 23° at a collision We number of 75. Here between 3 and 5 satellite droplets are produced, where the smallest size is about $30 \mu\text{m}$. Hence, the selected spatial resolution was sufficient for estimating the ligament size between separating droplets and the number and size of the satellite droplets for the present range of We numbers.

The impact parameter was modified by using the aliasing method (frequency shift, Gotaas et al. 2007b), and relative velocity variations in the range of $0.5\text{--}3.5 \text{ m/s}$ were achieved by a modification of the position angle between both droplet chains. For each position angle orientation of the nozzles, yielding a certain relative velocity and hence Weber number, the impact parameter was continuously varied between 0 and 1 by the frequency variation at one nozzle. This results in bands of data shown in Figs. 5 and 6 for almost constant We. After changing the orientation angle, the next series of measurements was conducted. More details on the image processing and data evaluation are provided by Kuschel and Sommerfeld (2013).

Image processing was performed in the following way. First the images were enhanced by applying gradient and

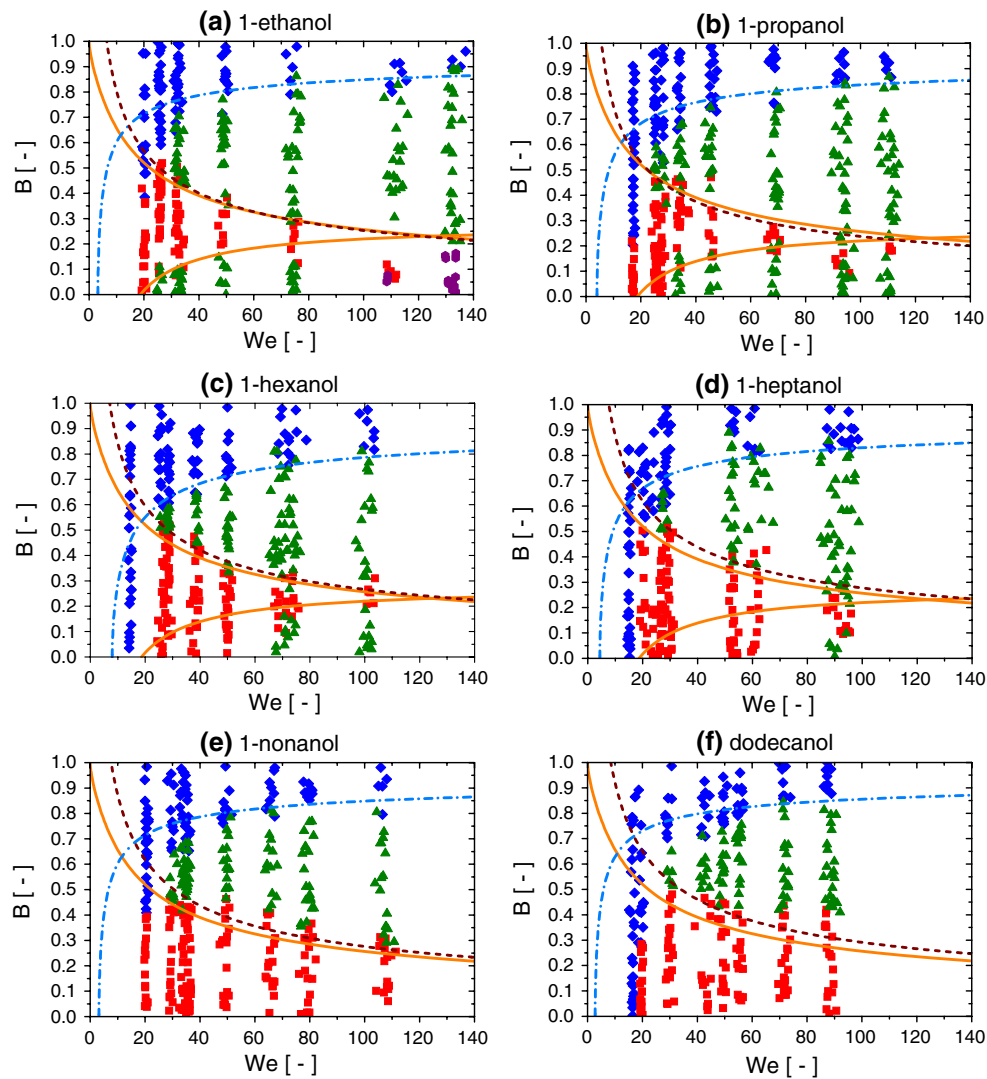


Fig. 5 Droplet collision maps for the series of alcohols; *squares (red)*: coalescence; *diamonds (blue)*: bouncing; *triangles (green)*: separation; *circles (purple)*: splashing; *solid line*: models of Ashgriz and Poo (1990); *dashed line*: model of Jiang et al. (1992) with the

constants $C_a = 2.454$ and $C_b = 0.102$; *dashed-dotted line*: model of Estrade et al. (1999) with shape factor according to Table 2 (note that the boundary line for reflexive separation is omitted if this phenomenon is not observed)

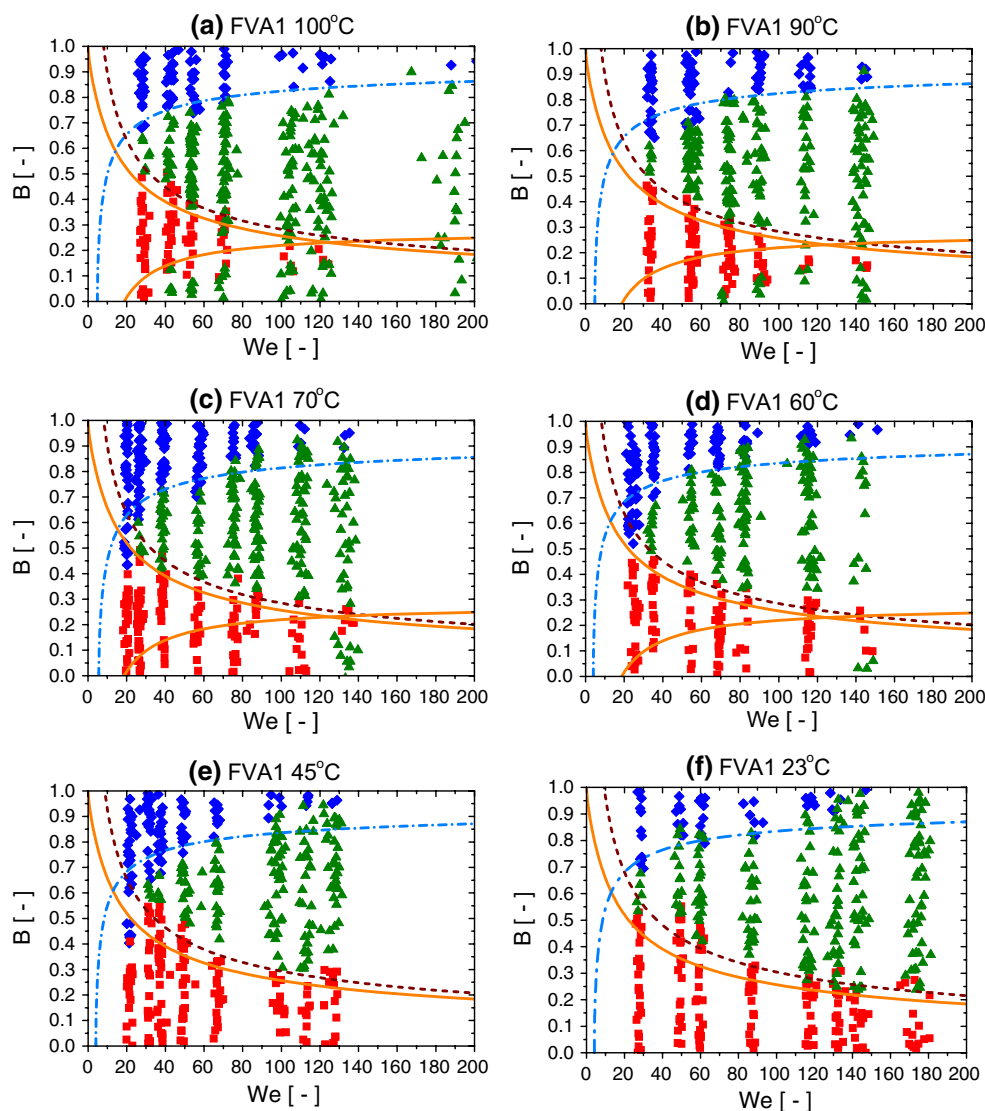
binarisation filters. The sharp edges of the droplets and liquid fragments were detected and transformed into positions on the image. Therefrom the centroids of the droplets were determined and the droplet diameters were calculated. The instantaneous droplet velocities were determined tracking their centroids on subsequent images (Kuschel and Sommerfeld 2013). Since it is not very likely to detect exactly the instant of droplet impact, a particle tracking approach was adopted. Therefore, pairs of possible collision partners were tracked from farther away up to the instant of contact (i.e. touching of the contours). For particle tracking and velocity determination an extended particle tracking velocimetry (PTV) approach was used. The tracking of the droplet pairs is not done with the instantaneous droplet

velocity, however, with the averaged droplet velocity of the respective chains (Kuschel and Sommerfeld 2013). All the data yielded the impact parameters and the Weber numbers for each collision event, and each individual collision event results in one symbol in Figs. 5 and 6.

4.1 Droplet substances

Previous studies were done for solution droplets with different solids content, i.e. polyvinylpyrrolidone (PVP K17 and PVP K30) and sucrose yielding dynamic viscosities in the range between 1 and 60 mPa s. Here it was shown that the location of the triple point in the collision map (bouncing, coalescence and stretching separation coincide) is

Fig. 6 Droplet collision maps for FVA1 reference oil at certain temperatures; *squares (red)*: coalescence; *diamonds (blue)*: bouncing; *triangles (green)*: separation; solid line: models of Ashgriz and Poo (1990); *dashed line*: model of Jiang et al. (1992) with the constants $C_a = 2.787$ and $C_b = 0.030$, *dashed-dotted line*: model of Estrade et al. (1999) with shape factor according to Table 2 (note that the boundary line for reflexive separation is omitted if this phenomenon is not observed)



depending in a continuous way on the dynamic viscosity and hence Ohnesorge number. For extending the database on droplet collision outcomes additional experiments were conducted for the series of alcohols and the reference oil FVA1 (see Table 1). The different alcohols have viscosities between 1.2 and 15.9 mPa s for a temperature of 22.0 °C. In the case of FVA1 reference oil the dynamic viscosity was varied between 3 and 28 mPa s by heating the oil to temperatures between 100 and 23 °C (see Table 1). For that, the pressure vessel was heated to 80% of the final temperature and two additional heating elements inside each nozzle allowed to establish the final temperature. For both substances increasing viscosity is coupled with growing surface tension from about 22 to 30 mN/m. Therefore, the Ohnesorge number also continuously increases for both species classes using the respective droplet sizes. This growth is more pronounced for the

reference oils since here the viscosity rise is stronger (Table 1).

5 Results and discussion

For allowing detailed modelling, complete collision maps are required resolving all boundaries between the different collision scenarios as well as the location of the triple point and the critical Weber number. In a previous study collisions of solution droplets were experimentally analysed and collision maps were presented for a range of solids contents and hence dynamic viscosities (Kuschel and Sommerfeld 2013). For generalising the resulting findings additional experiments for two pure fluids each with a range of viscosities were conducted for providing complete collision maps.

Table 1 Species data of the series of alcohols and of the reference oil at discrete temperatures

Type of liquid	μ (mPa s)	σ (mN/m)	ρ (kg/m ³)	Oh (–)
<i>Alcohols</i>				
Ethanol	1.2 ^a	22.6 ^a	790 ^a	0.015
1-Propanol	1.98 ^b	23.7 ^b	803 ^b	0.024
1-Hexanol	4.3 ^c	25.9 ^d	814 ^d	0.049
1-Heptanol	7.4 ^d	27.7 ^d	820 ^d	0.0813
1-Nonanol	12.9 ^b	28.0 ^b	828 ^b	0.1405
Dodecanol	15.9 ^c	30.4 ^f	831 ^f	0.1656
<i>Reference oil FVA1</i>				
100 °C	3.04	22.6	803.7	0.0364
90 °C	3.6	23.9	810.8	0.0417
70 °C	5.3	26.2	825.0	0.0581
60 °C	6.7	27.2	832.2	0.0718
45 °C	14.5	28.1	842.9	0.152
23 °C	28.2	30.3	858.5	0.282

^a Estrade et al. (1999), ^b Database BASF (2012), ^c Matsuo and Makita (1989), ^d Pinero et al. (2006), ^e Database-lookchem (1/2012), ^f Database-WolframAlpha (2/2012)

Table 2 Adapted values of the shape factor for the lower boundary of bouncing (Estrade et al. 1999) for the series of alcohols and the reference oil FVA1

Type	Species (°C)	Ψ	Type	Species	Ψ
Reference oil FVA1	100	3.6	Alcohols	Ethanol	3.4
	90	3.6		1-Propanol	3.5
	70	3.7		1-Hexanol	3.8
	60	3.3		1-Heptanol	3.5
	45	3.5		1-Nonanol	3.4
	23	3.4		Dodecanol	3.3

5.1 Collision maps

In this paragraph the collision maps (i.e. $B = f(We)$) for the series of alcohols and FVA1 reference oil will be presented. Because of the large parameter field relevant for droplet collisions here only the effect of viscosity in combination with surface tension has been investigated. The increase of both viscosity and surface tension results in an appreciable rise of the Oh number (Table 1). Other parameters like diameter ratio or ambient gas properties have been kept constant for the present experiments. All common collision scenarios (Fig. 1) were also observed in the present study, but for the case of ethanol splashing occurred as an additional outcome for small impact parameters and high Weber numbers (see Fig. 5) which is mainly the result of the low surface tension (see Table 2). The collision maps for the series of alcohols (Fig. 5) are ordered with

respect to increasing dynamic viscosity as summarised in Table 1. Most remarkable is the shift of the reflexive separation regime to the right towards higher Weber numbers which eventually for nonanol and dodecanol moves out of the considered We range. Since the viscosity variation is not very large, the region of stretching separation is only slightly shifted upward and to the right. This will become clearer when the movement of the triple point (i.e. onset of stretching separation) will be presented below. Both effects regarding separation increase the area of droplet coalescence, which mainly occurs for $B < 0.5$. For all cases bouncing seems to exist down to small impact parameters for low Weber number. Unfortunately, data in this region are missing for ethanol and nonanol. The effect of viscosity and surface tension on the lower boundary of bouncing at higher We is also very pronounced. First this boundary moves rapidly downward (see the result for hexanol) and then with further increasing viscosity moves upward again.

For better illustrating the movement of the collision outcome domains for the series of alcohols also the boundary lines between stretching separation and coalescence as well as coalescence and reflexive separation proposed by Ashgriz and Poo (1990) are included (Fig. 5). The region of reflexive separation is only captured reasonably well for ethanol and propanol with the low viscosity. With further increasing viscosity the theoretically derived boundary reflexive separation/coalescence of course is not able to predict the shift to the right, as it was derived for water only and does not account for viscosity effects (see Appendix 1). The boundary line for stretching separation/coalescence performs fairly well for all alcohols considered here. The model of Jiang et al. (1992), however, is able to describe the slight upward shift of the region of stretching separation with increasing viscosity much better. This was achieved by using an optimised parameter set of the model constants which was found for all alcohols by means of a least square method yielding values of $C_a = 2.454$ and $C_b = 0.102$ (the original model constants for water were $C_a = 2.33$ and $C_b = 0.41$, Jiang et al. 1992). The model of Estrade et al. (1999) to describe the lower boundary of bouncing was adapted through the shape parameter separately for each of the alcohols (see Table 2). Nevertheless, the model is able to capture the measured boundary only for higher Weber numbers (i.e. above $We \approx 30$ –40). Below these Weber numbers the model completely fails and cannot be suggested to be applied in this region.

The series of experiments with the reference oil FVA1 were sorted in such a way that the smallest viscosity was plotted first (Fig. 6). This allows a better comparison to the collision maps for the series of alcohols. In the case of the reference oil similar trends as for alcohols as well as for the PVP K30, PVP K17 and sucrose (Kuschel and Sommerfeld 2013) were observed; however, the onset of stretching

separation (i.e. triple point location) takes place at considerably higher impact parameters than for the alcohols. A reason for that might be the different structures of the molecules influencing the bulk behaviour of the liquid upon collision. While the series of alcohols consists only of short carbon chains with a functional group, the oil is composed of thousands of carbon atoms. This is also consistent with the results for PVP K30 reported by Kuschel and Sommerfeld (2013). Long polymers seem to show similar collision behaviour. Another obvious reason for the upward shift of the triple point to larger B values may be associated with the growth of the surface tension (see Table 1).

Moreover, bouncing is not observed for very small impact parameters in the case of the reference oils compared to the series of alcohols. Consequently, the fraction of bouncing within the investigated Weber number regime is smaller for the reference oil than for the series of alcohols. For the higher viscosity oils (i.e. lower temperature) bouncing collisions even disappear at high We numbers of around 140 (see Fig. 6e, f). Also for the reference oil FVA1 the region of reflexive separation is shifted to higher Weber numbers with increasing viscosity and eventually moves out of the considered domain. Again the different boundary models are compared with the experimental observation. The models of Ashgriz and Poo (1990) fail to correctly predict the boundaries of separating collisions, and the boundary line stretching separation/coalescence is for all viscosities located below the experimental boundary. The reflexive separation boundary is only acceptable for the lowest viscosity at 100° . The model of Estrade et al. (1999) for the lower bouncing boundary is only fitting the experimental data for intermediate Weber numbers, although the shape parameter was adjusted for each case (see Table 2). Finally, the Jiang et al. (1992) model was again adapted with one set of model parameters for the reference oils with different temperature (i.e. $C_a = 2.787$ and $C_b = 0.030$). With these settings the boundary between coalescence and stretching separation is predicted very well for all oil viscosities. Nevertheless, the model is still not predictive and experimental data are needed to determine the optimal set of model parameters. Therefore, in the following an approach is introduced whereby the model parameters can be evaluated based on the relaxation velocity and consequently is generalised with respect to the influence of viscosity and surface tension on the collision outcome.

For illustrating the effect of viscosity and surface tension which partly also may explain the shift of the triple point, a low and high viscous system is considered, namely the reference oil FVA1 at 100 and 23°C with an intermediate Weber number of $We \approx 50$. In Figs. 7 and 8 the different collision scenarios are shown for both viscosity cases. At low viscosity the surface of the droplets and liquid fragments after collision appear more ragged, which is

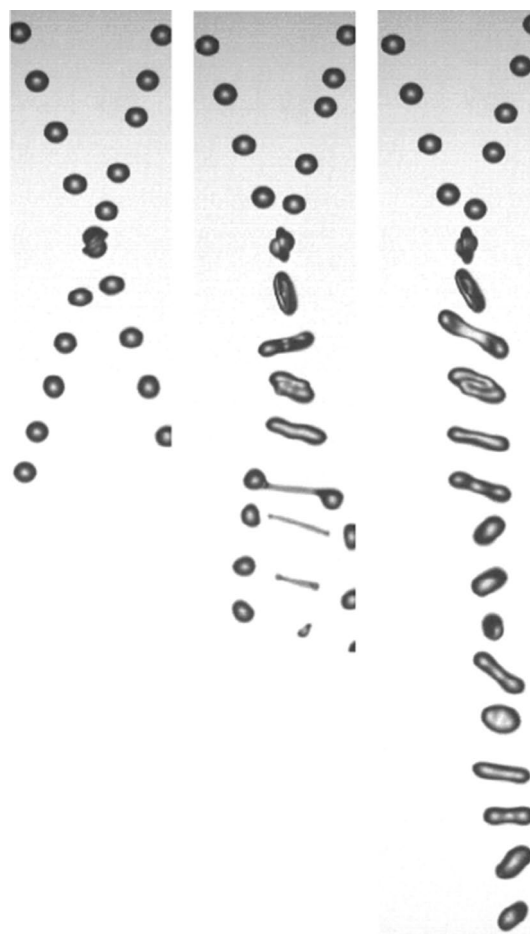


Fig. 7 Typical images of droplet collisions for the reference oil FVA1 with a temperature of 100° ; dynamic viscosity 3.04 mPa s ; droplet diameter $365\ \mu\text{m}$; $Oh = 0.0364$ (collision We number about 50), *left* bouncing collision, *middle*: separation, *right* coalescence

especially pronounced for stretching separation and coalescence (Fig. 7). This is first of all the effect of surface tension which is rather low and hence not strong enough to keep the surface smooth. Second, the damping of the droplet internal motion is lower due to the low viscosity which becomes very clear in the coalescence case where multiple oscillation periods are observed. This is not the case at higher viscosity (Fig. 8). In addition, stretching separation is going along with much smoother surfaces and very thin ligaments develop for higher viscosity and surface tension (i.e. higher Ohnesorge number) as already observed previously for solution droplet (Kuschel and Sommerfeld 2013). Moreover, for the low viscosity case a rim develops just after the droplets collided (see Fig. 7) which is most probably caused by the collision-induced internal flow. This rim is not visible for the high viscosity case (Fig. 8), as the internal flow is not that strong due to viscous damping. Such effects, however, may be only analysed by applying DNS (direct numerical simulations) as, for example, done

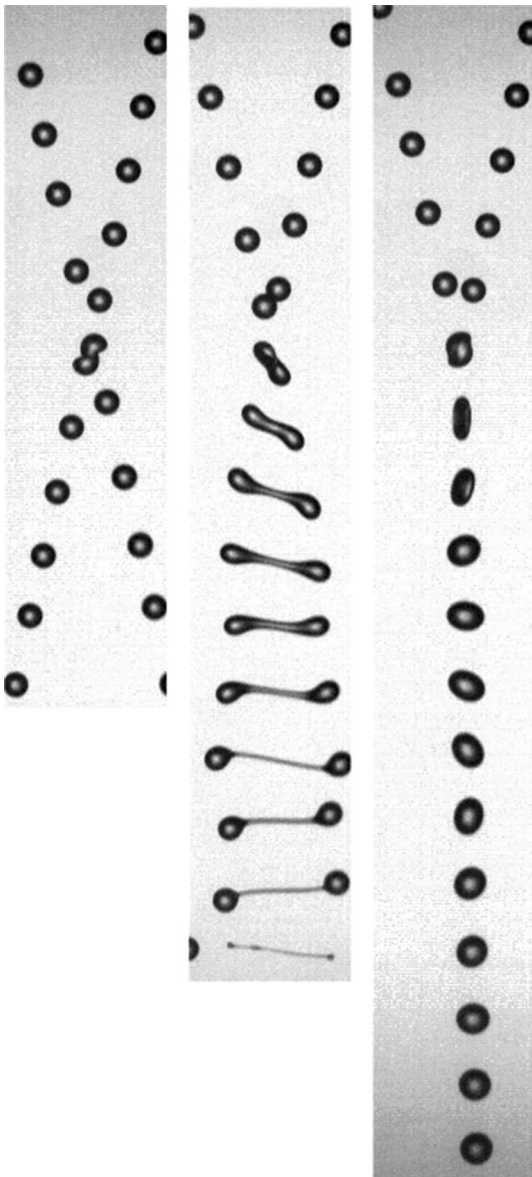


Fig. 8 Typical images of droplet collisions for the reference oil FVA1 with a temperature of 23°; dynamic viscosity 28.2 mPa s; droplet diameter 385 μm ; $Oh = 0.282$ (collision We number about 50), *left* bouncing collision, *middle* separation, *right* coalescence

by Focke et al. (2013) for studying the collision of droplets with different viscosity.

5.2 Onset of separation

In this section two newly derived correlations for the onset of reflexive and stretching separation will be presented. Therefore, additionally the results of Kuschel and Sommerfeld (2013) will be used and combined with the present results in order to have a larger variety of species with totally different chemical and physical properties.

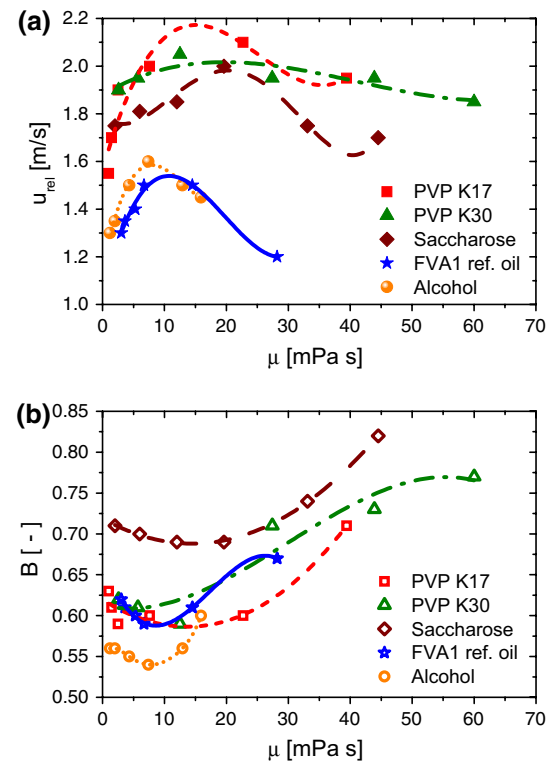


Fig. 9 Onset of stretching separation (i.e. location of triple point) for all different substances with respective trend lines: (red) dashed-short: PVP K17; (green) dashed-dotted: PVP K30; (brown) dashed: sucrose; (blue) solid: FVA1 reference oil; (orange) dotted: series of alcohols; **a** relative velocity at the onset of stretching separation, **b** impact parameter at the onset of stretching separation (triple point location)

First, the location of the triple point, i.e. the location for the beginning of stretching separation, was analysed for all substances considered. Either these points were directly taken out of the collision maps, or trend lines of the regime boundaries were used to identify the triple point. Therefore, continuous curves for the relative velocity and the impact parameter required to disrupt the surface of the droplets during collision in dependence of dynamic viscosity were found for all classes of substances (see Fig. 9). For deriving these plots the We number and the impact parameter at the triple point location were determined from the experiment and the relative velocity was calculated with the different properties for each species. With respect to the relative velocity in dependence of viscosity a clear maximum could be found for all liquid classes, whereas a minimum exists for the impact parameter. Actually, the correlation between normalised impact parameter and relative droplet velocity upon impact was already used by Planchette et al. (2012) for characterising the onset of stretching separation. Depending on the type of liquid the maximum/minimum of the curves is more or less pronounced and its location

is obviously depending on the type of liquid considered. Regarding the dependence of the relative velocity on the dynamic viscosity, the surface tension effect becomes obvious (Fig. 9). For the liquid systems PVP K17, PVP K30 and sucrose (surface tension around 70 mN/m) the onset of separation occurs clearly at higher relative velocities than for the alcohols and the reference oil FVA1 (surface tension around 25 mN/m). Hence as expected, higher impact energy is needed to disrupt the droplets if the surface tension is larger since surface energy tries to hold the droplets together.

A detailed analysis of the different curves revealed that the maximum of u_{rel} and the minimum of B are located at about the same relaxation velocity of $u_{\text{relax}}^* = (\sigma/\mu)^* = 3.51$ m/s, called critical relaxation velocity (see definition of the Capillary number Eq. 4), for all the considered substances. At this location the Capillary number takes value of about $Ca = 0.577$, which corresponds to an Ohnesorge number of $Oh = 0.115$. The relaxation velocity is a measure of the relative importance of surface tension and dynamic viscosity. Surface tension tends to produce the smallest surface area, which is hindered by viscosity. For relaxation velocities larger than the critical value the collision process and the outcome is governed by surface tension, whereas at smaller relaxation velocities viscosity largely influences the collision process (right of the maximum in Fig. 9a). Hence, one may define a surface tension- and viscosity-dominated regime for characterising the droplet behaviour upon collision as done by Blei and Sommerfeld (2007). This conclusion is also supported by the observation of satellite droplet formation. When separation is occurring, the viscosity-dominated regime is characterised by very long and thin ligaments which break up into a large number of very small satellite droplets (Kuschel and Sommerfeld 2013). On the other hand, in the surface tension-dominated regime (values left of the maximum in Fig. 9a) short and rather thick ligaments were created, breaking up into a few and larger droplets.

Before correlations for the onset of both separation regimes will be presented, a similarity number adopted from Naue and Bärwolff (1992) will be introduced, namely the structure parameter K , which is defined as (see Appendix 2):

$$K^n = \left[2\pi \left(1 + \frac{e-1}{6e} \right) \right]^n$$

$$K^1 = 6.9451 \quad (7)$$

Due to the fact that the book of Naue and Bärwolff (1992) is written in German, a more detailed explanation of the development of this structure parameter K is given

in Appendix 2. The parameter results from a flow process evaluation by means of information theory, declaring that natural processes try to organise themselves so that an optimal momentum and energy partitioning is achieved. Here structures are created on a macroscale originating from optimal self-organisation in the microscale. The K -parameter has been identified to characterise critical transition states found for several processes in fluid dynamics. Hence, different exponents of K denote critical states in a system possessing different degrees of freedom.

For example, $K^3 = 335$ is the critical Weber number for bubble break-up, whereas $K^4 = 2326.6$ represents the Reynolds number at which the transition from laminar to turbulent pipe flow occurs. Hence, also the onset of separation is such a transition process strongly governed by internal liquid motion and vortex development, both being affected by viscosity. The parameter K was used in the correlations to be introduced below for the triple point location as well as in the critical value of the Weber number, which describe either the onset of separation or the alteration of the dominating phenomenon (i.e. surface tension- or viscosity-dominated). Hence, universal collision maps (at least with regard to viscosity and surface tension effects) will be developed on the basis of the location of the triple point and the critical Weber number at $B = 0$ (see Fig. 1) making use of the structure parameter K . As will be shown below, the selected approach allows deriving correlations which very well predict the triple point location and the location of the onset of reflexive separation.

In order to generalise the onset of stretching separation all the data for the triple point location are summarised in a diagram $Re = f(Ca)$. Here the Reynolds number is the appropriate non-dimensional parameter since the process of stretching separation is mainly governed by the sliding of two liquid surfaces and hence depends on the ratio of inertia to viscous forces. The Capillary number is the ratio of the relative velocity between colliding droplets to the relaxation velocity (Eq. 4). In this double-logarithmic plot all the data for the triple point location from the present study are nicely arranged in a narrow band along one line (Fig. 10). Data from the literature is quite rare, only those of Qian and Law (1997) could contribute to the diagram; whereas in the work of Jiang et al. (1992), Estrade et al. (1999) and Gotaas et al. (2007b) not sufficient information is available to calculate Capillary numbers. For the case of tetradecane droplet collisions reported by Qian and Law (1997) a Capillary number can be estimated for the 1 bar nitrogen atmosphere. In the publication of Jiang et al. (1992), where other alkanes are considered, the location of the triple point could not be determined. Here only the region of coalescence was

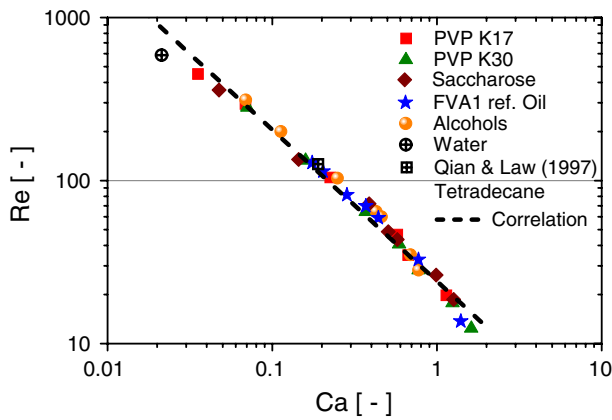


Fig. 10 Onset of stretching separation or triple point location for different substances and systems; (red) squares: PVP K17; (green) triangles: PVP K30; (brown) diamonds: sucrose; (blue) stars: FVA1 reference oil; (orange) circles: series of alcohols; (crossed circle): water; (crosses square): tetradecane in nitrogen at 1 bar (Qian and Law 1997); dashed line: correlation Eq. 8

demarcated, and no boundary lines between bouncing and stretching separation were provided.

Eventually, all the available data points may be fitted by a single correlation incorporating the structure parameter K (Eq. 7) as shown in Fig. 10.

$$Re = \frac{K^2}{2} Ca^{-\sqrt{1-\frac{1}{\epsilon^2}}} \quad (8)$$

Therefore, it is now possible to specify the Weber number necessary for yielding stretching separation by simply introducing $Re = We/Ca$ in Eq. 8. Left of the correlation curve in Fig. 10 coalescence and bouncing may occur, while bouncing, coalescence and stretching could happen on the right-hand side (see Figs. 5, 6). For the estimation of the triple point Weber number in dependence of only the liquid properties and the droplet diameter one may be rearranged Eq. 8 to obtain:

$$We = \left(\frac{K^2}{2}\right)^{\frac{2}{1+\sqrt{1-1/\epsilon^2}}} Oh^{2\frac{1-\sqrt{1-1/\epsilon^2}}{1+\sqrt{1-1/\epsilon^2}}} \quad (9)$$

For distinguishing between the different collision outcomes, theoretically derived boundary lines are needed which have to be adapted in order to capture the shift of the regimes resulting from the variation of the liquid properties. The boundary line between stretching separation and coalescence was developed based on the model of Jiang et al. (1992) which the only model is accounting for viscous dissipation. This model includes two parameters which are not universal and therefore have to be adapted (see Kuschel and Sommerfeld 2013). Consequently, the boundary line according to Eq. 18 was fitted to the measured boundary between coalescence and stretching separation for all the fluids considered by a least square method (see, e.g., Figs. 5, 6). Here it was also ensured

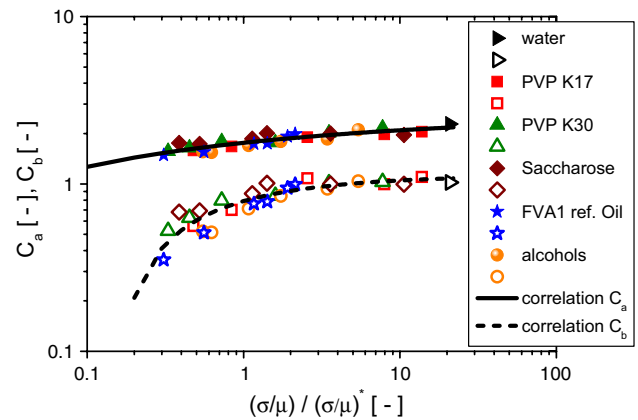


Fig. 11 Illustration of the optimal Jiang parameters for all species investigated in dependence of the ratio $u_{relax}/u_{relax}^* = (\sigma/\mu) / (\sigma/\mu)^*$ together with the correlation curves (black closed line: C_a ; black dashed line: C_b , both according to Eq. 10; closed symbols C_a data; open symbols C_b data; triangles right (black) water; squares (red) PVP K17; triangles (green) PVP K30; diamonds (brown) sucrose; stars (blue) FVA1 reference oil; circles (orange) series of alcohols ($u_{relax}^* = (\sigma/\mu)^* = 3.51$ m/s)

that the curves go through the point of beginning stretching separation predicted by correlation Eq. 9. Plotting now all data for the two model parameters obtained from the fitting procedure versus the relaxation velocity normalised by the critical relaxation velocity one obtains rather narrow bands of data points for all the substances considered in this work (i.e. water, PVP K17/K30, sucrose, alcohols and reference oil FVA1) as shown in Fig. 11. In order to obtain the model parameters C_a and C_b the following correlations are found to fit these data for dynamic viscosities between 1 and 60 mPa s and surface tensions between 20 and 77 mN/m (Fig. 11):

$$C_a = 2.762 - \left(\frac{u_{relax}}{u_{relax}^*}\right)^{-0.175}$$

$$C_b = 1.134 - 0.345 \left(\frac{u_{relax}}{u_{relax}^*}\right)^{-0.613} \quad (10)$$

The next step in the modelling is the description of the onset of reflexive separation for $B = 0$, the so-called critical Weber number. As it was observed previously (Kuschel and Sommerfeld 2013) and also here for alcohols and the reference oil FVA1, increasing viscosity yields a shift of this critical point to the right towards larger We . For describing the shift of the onset of reflexive separation Gotaas et al. (2007a, b) proposed to use the dependence of the Weber number on the Ohnesorge number (Fig. 12a). Using literature data as well as all the present data and those presented by Kuschel and Sommerfeld (2013) it becomes obvious that the points show a relatively large scatter around the segmented correlations proposed by Gotaas et al. (2007a, b).

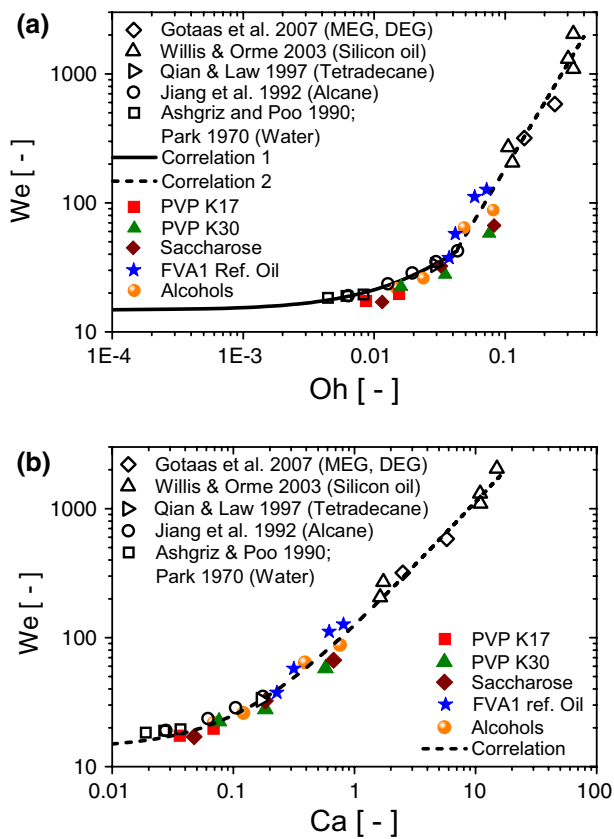


Fig. 12 Onset of reflexive separation for different systems (critical point) and literature data compared with proposed correlations; **a** onset of reflexive separation proposed by Gotaas et al. (2007a, b); correlation 1: $We = 643 Oh + 14.8$; correlation 2: $We = 9309 Oh^{1.7056}$; **b** new correlation to describe the onset of reflexive separation, critical point (Eq. 11)

Since head-on collisions of two droplets are largely affected by deformation processes, it is more logical to use the Capillary number which is the ratio of viscous forces to surface tension forces. In such a diagram (i.e. $We = f(Ca)$, Fig. 12b) the scatter of the data points is smaller and they can be matched very good by one linear correlation, again formulated in terms of the K -number (Naue and Bärwolff 1992):

$$We_{crit,B=0} = \frac{K^3}{3} Ca + 2 K \tag{11}$$

Also the data from the literature having higher capillary numbers are very well represented by this correlation. In modelling now the boundary line between reflexive separation and coalescence, the correlation developed by Ashgriz and Poo (1990) is taken and just shifted to the right by the critical Weber number obtained from Eq. 11. Although this model does not explicitly account for viscosity effects, this is a practical way since the experimental studies presented here and by Kuschel and Sommerfeld (2013) showed that the

extent of the reflexive separation regime to higher B values is always comparable for the liquids considered. This eventually yields the following equation for the boundary line:

$$We = (We_{crit} - We_{crit,water}) + 3 \left[7(1 + \Delta^3)^{2/3} - 4(1 + \Delta^2) \right] \times \frac{\Delta(1 + \Delta^3)^2}{\Delta^6 \eta_S + \eta_L} \tag{12}$$

where We_{crit} is obtained from the correlation in Eq. 11 and $We_{crit,water}$ is the critical value for water as originally derived ($We_{crit,water} = 18.67$). The parameters η_S and η_L are given by Eq. 17.

In the following the role of the K -number, with which it is possible to describe the onset of separation just with the help of optimal processes, will be investigated. If one compares the pre-factors of the Capillary number in Eqs. 8 and 11, a general law for the onset of separation can be formulated as:

$$K^* = \frac{\left[2\pi \left(1 + \frac{e-1}{6e} \right) \right]^n}{n} = \frac{K^n}{n} \tag{13}$$

For the case of the stretching separation an additional parameter occurs, which indicates that the degree of freedom is sufficient to allow for the development of optimal processes. The exponent of the Capillary number, which was borrowed from Eq. 27, fits very well all considered experimental data. While for the onset of stretching separation only a two-dimensional process in the phase space is necessary, reflexive separation requires a larger energy (higher effort), with the result that the process consists of 3 dimensions. This means that structures of higher dimension are essential to enforce reflexive separation processes.

For a complete description of the collision outcome with the help of the collision map, it would be also necessary to have a correlation for the lower boundary of the occurrence of bouncing. In Figs. 5 and 6 this was tried on the basis of the model of Estrade et al. (1999) by adapting the shape factor included in Eq. 19. However, so far no generalisation of the shape factor was possible. The shape factors used in Figs. 5 and 6 are summarised in Table 2. It is obvious that the Estrade et al. (1999) model matches the boundary reasonably well for higher Weber numbers. In the region around and below the triple point the model, however, mostly fails, indicating that a further analysis of the model is required.

6 Model validation

Finally, all the elements of the above-described models are put together and applied to systems with pure liquids and

solutions with varying dynamic viscosity for validation. In each case the experimentally obtained data are shown together with the proposed boundary models. For the Jiang et al. (1992) model the parameters according to Eq. 10 are used and the line begins at the triple point (from Eq. 9). The Ashgriz and Poo (1990) model was shifted by the value of the critical We number (Eq. 11) to the right, which showed to be a reasonable approximation. Finally, the Estrade et al. (1999) model was individually adapted with the shape factor to match the boundary between bouncing and stretching separation as well as coalescence. The applied shape factors are provided also in the figure captions.

For the alcohols all the boundary lines fit very well to the experimental results for both viscosities shown here (Fig. 13). Also the domain of reflexive separation occurring for hexanol is captured very well. The model for the bouncing boundary matches the experiments above the triple point quite good, but completely fails in the region below.

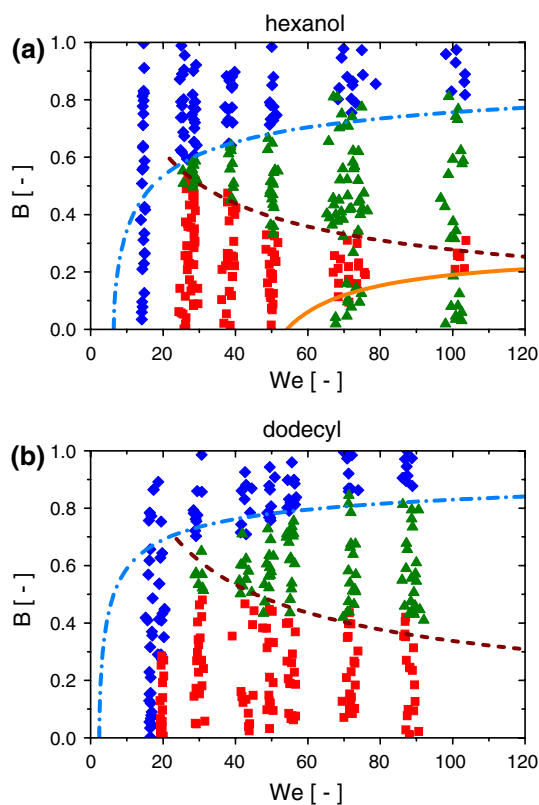


Fig. 13 Application of the new hybrid model and comparison with measurements; **a** hexanol ($\mu = 4.3$ mPa s, $Oh = 0.049$); **b** dodecanol ($\mu = 15.9$ mPa s, $Oh = 0.1656$); (blue) diamonds: bouncing, (red) squares: coalescence, (green) triangles: stretching and reflexive separation (note the lower cluster of triangles belongs to reflexive separation only); dashed (brown) line: enhanced model of Jiang et al. (1992) using Eqs. (8 and 9); (orange) closed line: extended model of Ashgriz and Poo (1990) using Eqs. (11 and 12) and (light blue) dash-dot line: adapted Estrade et al. (1999) model according to Eq. 19 with shape parameters $\Psi_{\text{Hexanol}} = 3.8$ and $\Psi_{\text{Dodecanol}} = 3.3$

For both higher-viscous alcohols bouncing is observed down to $B = 0$ and almost up to a Weber number of 20. The model predicts a much narrower region of bouncing going from the triple point down to $B = 0$.

The reference oil FVA1 at 60° and 23° is shown in Fig. 14. The boundary line stretching separation/coalescence reflects the measurements very good, and the location of the triple point is captured. The critical Weber number resulting from the model is much lower compared to the experimental observation, and hence, the region of reflexive separation is over-predicted. This is of course associated with the relative large scatter of the data points around the correlation (Eq. 11) as shown in Fig. 12b). Bouncing seems to disappear completely in the case of FVA1 at larger Weber numbers, which is expectedly not captured by the model. Below the triple point not sufficient experiments are available for judging the quality of the bouncing boundary line.

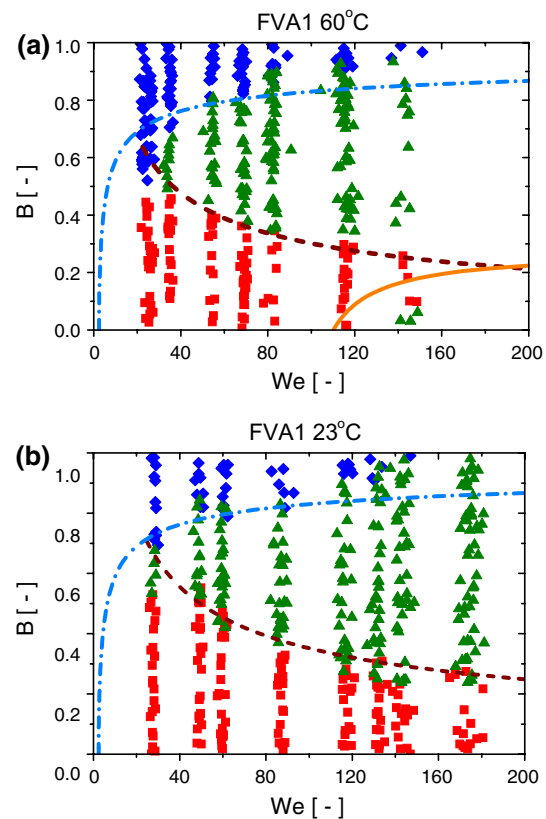


Fig. 14 Application of the new hybrid model and comparison with measurements; **a** FVA1 60° ($\mu = 6.7$ mPa s, $Oh = 0.0722$); **b** FVA1 23° ($\mu = 28.2$ mPa s, $Oh = 0.2818$); (blue) diamonds: bouncing, (red) squares: coalescence, (green) triangles: stretching and reflexive separation (note: the lower cluster of triangles belongs to reflexive separation only); dashed (brown) line: enhanced model of Jiang et al. (1992) using Eqs. (8 and 9); (orange) closed line: extended model of Ashgriz and Poo (1990) using Eqs. (11 and 12) and (light blue) dash-dot line: adapted Estrade et al. (1999) model according to Eq. 19 with shape parameters $\Psi_{\text{FVA1 } 60} = 3.3$ and $\Psi_{\text{FVA1 } 23} = 3.4$

The performance of the models applied to solution droplets is considered in the following. All boundaries obtained for PVP K30 reproduce the experiments satisfactorily which may be acceptable for spray dryer calculations (Fig. 15). The bouncing boundaries are in much better agreement with

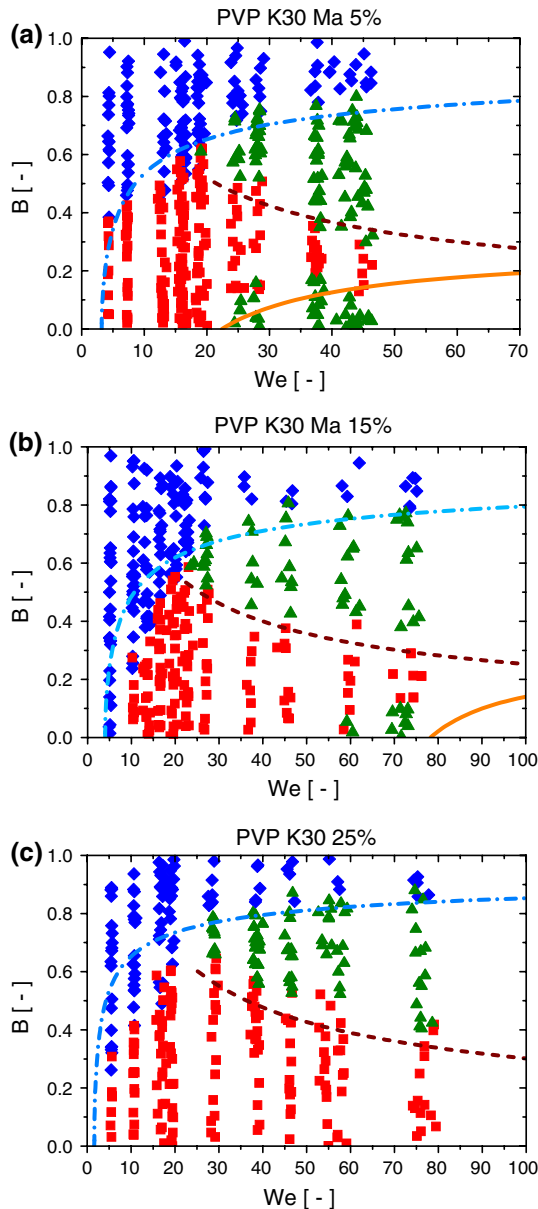


Fig. 15 Application of the new hybrid model and comparison with measurements; **a** PVP K30 5% ($\mu = 2.6$ mPa s, $Oh = 0.0158$); **b** PVP K30 15% ($\mu = 12.5$ mPa s, $Oh = 0.076$); **c** PVP K30 25% ($\mu = 60$ mPa s, $Oh = 0.365$); (blue) diamonds: bouncing, (red) squares: coalescence, (green) triangles: stretching and reflexive separation (note: the lower cluster of triangles belongs to reflexive separation only); dashed (brown) line: enhanced model of Jiang et al. (1992) using Eqs. (8 and 9); (orange) closed line: extended model of Ashgriz and Poo (1990) using Eqs. (11 and 12) and (light blue) dash-dot line: adapted Estrade et al. (1999) model according to Eq. 19 with shape parameters $\Psi_{K30\ 5\%} = 3.4$, $\Psi_{K30\ 15\%} = 3.5$ and $\Psi_{K30\ 25\%} = 3.2$

the data compared to the pure fluids, except for higher viscosity in the region of Weber numbers between 5 and 25 (Fig. 15b, c). The upward shift of the boundary between stretching separation and coalescence is correctly predicted by the new model although the triple point location is not exactly matched with respect to the Weber number. This again is connected with the scatter of the measurements around the proposed correlations for the triple point (Eq. 8) and the associated model parameters (Eq. 10). This is also the reason for not properly capturing the critical point.

As shown before (Kuschel and Sommerfeld 2013), sucrose exhibits the largest shift of the stretching separation coalescence boundary with increasing solids content and hence viscosity. This is reasonably captured by the physical model, but not perfectly (Fig. 16). Generally, the prediction is slightly below the experimental observation, and therefore, also the triple point location is not properly grasped. The bouncing boundary on the other hand is very well reflected.

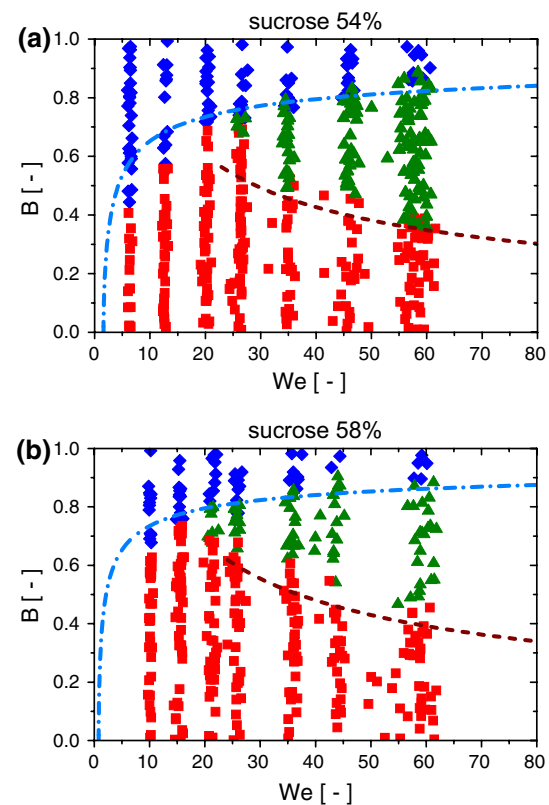


Fig. 16 Application of the new hybrid model and comparison with measurements; **a** sucrose 54% ($\mu = 19.4$ mPa s, $Oh = 0.1015$); **b** sucrose 58% ($\mu = 42.2$ mPa s, $Oh = 0.219$); (blue) diamonds: bouncing, (red) squares: coalescence, (green) triangles: stretching separation; dashed (brown) line: enhanced model of Jiang et al. (1992) using Eqs. (8 and 9) and (light blue) dash-dot line: adapted Estrade et al. (1999) model according to Eq. 19 with shape parameters $\Psi_{sucrose\ 54\%} = 3.2$ and $\Psi_{sucrose\ 58\%} = 3.1$

7 Conclusions

Droplet–droplet collisions for various solutions were experimentally studied in detail by Kuschel and Sommerfeld (2013). For extending this database with respect to fluid properties and viscosity and to allow for a more reliable modelling here additional experiments are presented for pure fluids. All these measurements cover a wide range of dynamic viscosities, namely between 1 and 60 mPa s. For that purpose two mono-sized droplet chains were produced by vibrating orifice droplet generators so that binary collisions could be accurately realised. So far only collisions of droplets with identical size and dynamic viscosity were considered. The outcome of the collision was recorded based on shadow imaging employing a high-speed camera. The applied image processing includes an enhancement of the images by several filter operations so that all droplet properties before and after collision could be reliably obtained incorporating also droplet fragments and satellite droplets.

On the basis of these results a universal composite model was developed for describing the location of characteristic points for the onset of separation (i.e. stretching and reflexive separation) in the classical collision map (i.e. $B = f(We)$). The location of the triple point (bouncing, stretching separation and coalescence meet) is expressed in terms of the relative velocity with respect to the viscosity and showed a characteristic behaviour with a distinct maximum. The dependence of the impact parameter B on the viscosity on the other hand showed a clear minimum. This implies a characteristic movement of the triple point with increasing viscosity; first the triple point moves to higher We and then goes back again slightly; second the triple point moves slightly down to smaller B and then is shifted up again to higher B . This eventually enlarges the regime of droplet coalescence. For all substances considered, this maximum and minimum was found at a relaxation velocity of about $(\sigma/\mu) \approx 3.51$ m/s. Droplet collisions with smaller values are dominated by viscosity, whereas larger values result in a stronger influence of surface tension. Hence, the relaxation velocity is a characteristic parameter for the droplet collision process. Regarding the onset of reflexive separation, it was found that the critical Weber number (i.e. for $B = 0$) moves to higher values with increasing viscosity and eventually was shifted out of the considered We regime for high viscous systems. Note the highest Weber number considered was about 180.

Based on a theory for optimal self-organisation of structures (structure parameter K , introduced by Naue and Bärowolf 1992) two correlations were developed which are feasible to predict the onset of separation for very different substances, namely pure fluids and solutions having a wide range of viscosities. The Capillary number proved to

be a very important non-dimensional similarity number to describe the onset of separation. The triple point location (i.e. onset of reflexive separation) was described by a correlation between Re and Ca which very well encompasses all experimental points from all substances considered. The critical Weber number (onset of reflexive separation) could be reasonably well correlated with Ca based on the K -parameter for the substances considered in this study as well as other literature data. However, the scatter of the experimental data around the correlation was somewhat large.

The new composite model uses both correlations in combination with two common boundary line models, namely that of Ashgriz and Poo (1990) and Jiang et al. (1992) to describe the boundaries between coalescence and stretching as well as reflexive separation and hence the extent of the coalescence regime. The two model parameters in the boundary model of Jiang et al. (1992) could be specified in terms of the normalised relaxation velocity. The reflexive separation boundary could be pretty well described by simply shifting the model of Ashgriz and Poo (1990) by the amount of the critical Weber number to the right (see Eq. 12).

The lower boundary of bouncing could be reasonably described by the model of Estrade et al. (1999), however, only if the involved shape parameter is adapted individually for each system considered. Hence, this model needs further theoretical analysis and improvement, especially for allowing better predictions of the bouncing/coalescence boundary for Weber numbers below the triple point.

For the considered substances the new composite modelling approach for describing the boundary lines between collision scenarios showed reasonable good agreement with the experimental results over the entire range of viscosities considered. For the first time it is now possible to determine the outcome of droplet collisions with acceptable accuracy for viscosities up to 60 mPa s, which is essential for spray calculation with an Euler/Lagrange approach. It should, however, be emphasised that the model so far only covers collisions with identical viscosity and droplet size. In general, the composite model predicts the different boundary lines relatively well with respect to the numerous experiments conducted. There are, however, some weaknesses which may be solved with further experimental studies and theoretical analysis.

- The bouncing boundary model was individually fitted and needs further elaboration and generalisation with regard to viscosity. For lower viscous substances the bouncing regime below $B \approx 0.5$ or below the triple point was not properly captured. For higher viscosities the model performs reasonably well.

- The location of the critical point was not always properly met, which is associated with a relatively large scatter of the data around the newly proposed correlation curve (Fig. 12b).
- Especially for the high viscous sucrose systems, the stretching separation/coalescence boundary was predicted to be located below the experiments and the triple point location was not matched perfectly. For yielding better agreement in this respect, the evaluation of the parameters in the Jiang et al. (1992) model needs to be improved.

Nevertheless, the newly proposed composite model is an important advancement in the prediction of the collision outcome for higher-viscous droplets. However, the study was limited to colliding droplets with identical viscosity and diameter. In practice, for example in combustion or spray drying, the droplets undergo size changes due to evaporation and are heated up, so that also the liquid properties and especially the dynamic viscosity may change strongly. This will need further detailed experimental studies.

Acknowledgements The authors acknowledge the financial support of this research project by the Deutsche Forschungsgemeinschaft (DFG) under contract SO 204/35-1 and 2. Furthermore, the supply of species data by the Technical University Freiberg within the DFG Priority Program SPP 1423 is acknowledged. Finally, the authors would like to thank Prof. Naeu for valuable discussions about his work and explanations on optimal processes.

Appendix 1: Collision boundary models

In this section a brief overview about the boundary line models used for deciding on the collision outcome by using collision maps of the form $B = f(We)$ will be given. Details on the derivation of the equations are given in the respective articles. These models will be also used for comparison with the present experimental data. It should be emphasised that in the present study the colliding droplet properties (i.e. size and substance) are identical and also the environmental conditions were not changed (i.e. air at ambient conditions).

Model of Ashgriz and Poo (1990)

Ashgriz and Poo (1990) developed two correlations for the boundaries of coalescence and separation. For off-centre collisions only a small portion of the droplets, depending on the impact parameter, come into contact and are partially deformed. This interaction region is stretched until it breaks up, creating satellite droplets. Based on an energy

balance the following equation for the boundary between coalescence and stretching separation was derived:

$$We = \frac{4(1 + \Delta^3)^2 [3(1 + \Delta)(1 - B)(\Delta^3 \phi_S + \phi_L)]^{1/2}}{\Delta^2 [(1 + \Delta^3) - (1 - B^2)(\phi_S + \Delta^3 \phi_L)]} \tag{14}$$

where

$$\phi_S = \begin{cases} 1 - \frac{1}{4\Delta^3}(2\Delta - \tau)^2(\Delta + \tau) & \text{for } h > 0.5d_S \\ \frac{\tau^2}{4\Delta^3}(3\Delta - \tau) & \text{for } h < 0.5d_S \end{cases}$$

$$\phi_L = \begin{cases} 1 - \frac{1}{4}(2 - \tau)^2(1 + \tau) & \text{for } h > 0.5d_L \\ \frac{\tau^2}{4}(3 - \tau) & \text{for } h < 0.5d_L \end{cases}$$

$$h = \frac{1}{2}(d_L + d_S)(1 - B) \tag{15}$$

and $\tau = (1 - B)(1 + \Delta)$ are the substitutes of the equation above.

Reflexive separation takes place for near head-on collisions. A torus-like collision complex is created with a thin lamella spanning the torus. After rebound of the liquid, it is stretched and a ligament is formed, which eventually breaks up, forming mostly one large satellite (Brenn et al. 2001). The criterion for reflexive separation is fulfilled, when the effective kinetic energy is larger than 75% of the nominal surface energy of the combined droplets:

$$We = 3 \left[7(1 + \Delta^3)^{2/3} - 4(1 + \Delta^2) \right] \frac{\Delta(1 + \Delta^3)^2}{\Delta^6 \eta_S + \eta_L} \tag{16}$$

The geometrical parameters given in Eq. (16) are:

$$\eta_S = 2(1 - \xi)^2 (1 - \xi^2)^{1/2} - 1$$

$$\eta_L = 2(\Delta - \xi)^2 (\Delta^2 - \xi^2)^{1/2} - \Delta^3$$

$$\xi = (1/2) B (1 + \Delta) \tag{17}$$

Model of Jiang et al. (1992)

In contrast to the model of Ashgriz and Poo (1990), the model of Jiang et al. (1992) accounts for viscous dissipation by applying momentum conservation. It has been developed to describe the boundary between coalescence and stretching separation. The final equation for the boundary curve contains two model constants (i.e. C_a and C_b) which can be fitted to the experimental data (see, e.g., Gotaas et al. 2007a, b):

$$B = \frac{C_a}{We^{1/2}} \left[1 + C_b \frac{\mu}{\sigma} \left(\frac{\rho d_1}{\sigma} \right)^{1/2} \right] \tag{18}$$

Model of Estrade et al. (1999)

This model has been derived from collision maps obtained experimentally for ethanol droplets and describes the lower boundary of bouncing. A free model constant, the shape factor Ψ (for ethanol the value was found to be 3.351), has been introduced whereby the model can be adapted to fit other droplet collision conditions:

$$We = \frac{\Delta(1 + \Delta^2)(4\Psi - 12)}{\chi(1 - B^2)} \tag{19}$$

where

$$\begin{aligned} \chi &= 1 - 0.25(2 - \tau)^2(1 + \tau) & \text{if: } \tau > 1 \\ \chi &= 0.25\tau^2(3 - \tau) & \text{if: } \tau \leq 1 \end{aligned} \tag{20}$$

and $\tau = (1 - B)(1 + \Delta)$ is an additional parameter given in Eq. 20.

Appendix 2

Summary of the model of Naue and Bärwolff (1992)

The model description is divided into two major parts. In the first part, the concept of process evaluation by means of the information entropy will be explained, and in the second paragraph the derivation of the K -numbers, which may be regarded as a structure parameter, will be presented.

Concept of process evaluation

The process of vortex development is characterised by a main flow transport and a lateral motion where the latter is feed by the convective flow. The non-dimensional entropy S is a measure of the partitioning of the two characteristic motions where joint entropy is maximised. For evaluating an exponential distributed property f , defined in the interval $0 < f \leq 1$, the non-dimensional entropy is used:

$$S = -\ln f \tag{21}$$

The entropy production σ can be derived from:

$$\frac{d\sigma}{df} = S \tag{22}$$

After an integration in the interval $f = f_*$ to $f = 1$ and the application of a Taylor series expansion a modified ansatz compared to the thermodynamic entropy definition is obtained. The result of the integration of Eq. 22 gives the entropy production:

$$\sigma_* - f_* = -f_* \ln f_* \tag{23}$$

The term $-f_* \ln f_*$ is called information entropy σ_{i*} and has been introduced by Shannon (1948) in cybernetics. With the averaged values f_* , σ_* and σ_{i*} in a residence range, the mean entropy production can be written as follows:

$$\tilde{\sigma}_* - \tilde{f}_* = \tilde{\sigma}_{i*} \tag{24}$$

The difference from the equation above is equal to the quality gain which is expressed by the information entropy. A process may be regarded as optimal, if the information entropy is maximised. Now a distinction between competing and sequential processes has been carried out, which is omitted here because of the large amount of equations.

Optimal processes and derivation of K

Processes in which the information entropy approaches a maximum are considered as optimal processes. Competing processes might have a phase shift to each other, which the authors (Naue and Bärwolff 1992) called phase₁ and phase₂ for a two-dimensional process. The maximum of the information entropy can be found by the derivation of the definition equation which yields:

$$\frac{d\sigma_{i*}}{df_*} = \frac{df_* \ln f_*}{df_*} = \ln f_* - 1 \tag{25}$$

For the optimum one obtains $\ln(f_{*opt}) = -1$ or $f_{*opt} = 1/e$ as a solution. The phase shift mentioned above can either be excited or weakened through convection or conduction effects, depending on the sign of phase_n. As a result of these considerations it may be concluded that for optimal processes, waves are optimal phase shifted to each other and develop optimal. In a two-dimensional phase space the values for the optimal phase functions are:

$$\text{phase}_1 = \frac{1}{e} \tag{26}$$

$$\text{phase}_2 = \left(1 - \frac{1}{e^2}\right)^{\frac{1}{2}} \tag{27}$$

The similarity number or structure parameter K (here called structure parameter) will be obtained by considering the interaction of structures (i.e. velocity fluctuations) with the mean flow. The transport of the structures results from the momentum distribution among competing processes. For that, the author considered a pipe flow and asked for the optimal partitioning of the total momentum to the convective transport and the structure movement for the three-dimensional case, with the result that only one meaningful solution for this ratio is obtained:

$$\phi = -\frac{e - 1}{2e} \tag{28}$$

The process of turbulent velocity fluctuations is of course fully three-dimensional. The momentum velocity v_j is a measure of the distance travelled in a certain time interval Δt . First it is assumed that the travelled distance is identical in all three directions in space (i.e. isotropic). Hence, a third of the additional travel distance is obtained from:

$$v_j \frac{e-1}{6e} \Delta t \quad (29)$$

The entire volume of the residence, without turbulent velocity fluctuations, within a certain cross-sectional area is given as $V_0 = v_j A_j \Delta t$. On the other hand, with turbulent velocity fluctuations, if the volume is assumed as isotropic, one obtains:

$$V_t = v_j A_j \Delta t \left(1 + \frac{e-1}{2e} \right) \quad (30)$$

Consequently, the volume ratio characterising the expansion due to velocity fluctuations is obtained from:

$$\frac{V_t}{V_0} = 1 + \frac{e-1}{2e} = \left(\frac{s_t}{s_0} \right)^3 \quad (31)$$

where s_0 and s_t are the lengths of the volume edges without and with turbulent fluctuations, respectively. A series expansion yields:

$$\frac{s_t}{s_0} = 1 + \frac{e-1}{6e} \quad (32)$$

The proposed structure parameter K characterises this expansion due to velocity fluctuations or vortex motion for a spherical volume:

$$K = 2\pi \frac{s_t}{s_0} = 2\pi \left(1 + \frac{e-1}{6e} \right) = 6.9451 \quad (33)$$

The final expression for the structure parameter for a n -dimensional process (i.e. dimensionality of the structures in the phase space) is given by:

$$K^n = \left[2\pi \left(1 + \frac{e-1}{6e} \right) \right]^n \quad (34)$$

References

- Ashgriz N, Poo JY (1990) Coalescence and separation in binary collisions of liquid drops. *J Fluid Mech* 221:183–204
- Blei S, Sommerfeld M (2007) CFD in drying technology-spray drying simulation. In: Tsotsas E, Majumdar AS (eds) *Modern drying technology: volume 1 computational tools at different scales*. WILEY-VCH, Weinheim, pp 155–208
- Brazier-Smith PR, Jennings SG, Latham J (1972) The interaction of falling water drops: coalescence. *Proc R Soc Lond A* 326:393–408
- Brenn G, Valkovska D, Danov KD (2001) The formation of satellite droplets by unstable binary droplet collisions. *Phys Fluids* 13:2463–2477
- Chen R-H (2007) Diesel–diesel and diesel–ethanol drop collisions. *Appl Therm Eng* 27:604–610
- Database-BASF (2/2012) http://www.loesemittel.basf.com/portal/6/de/dt.jsp?setCursor=1_224361&seite=alkohole_und_aldehyde/
- Database-lookchem (1/2012) <http://www.lookchem.com/Dodecyl-alcohol/>
- Database-WolframAlpha (2/2012) <http://www.wolframalpha.com/input/?i=1-Heptanol+/>
- de O Macedo T, Pereira RG, Pardal JM, Soqres AS, de de J Lameira V (2013) Viscosity of vegetable oils and biodiesel and energy generation. *Int Sch Sci Res Innov* 7:251–256
- Estrade J-P, Carentz H, Lavergne G, Biscos Y (1999) Experimental investigation of dynamic binary collision of ethanol droplets—a model for droplet coalescence and bouncing. *Int J Heat Fluid Flow* 20:486–491
- Focke C, Kuschel M, Sommerfeld M, Bothe D (2013) Collision between high and low viscosity droplets: direct numerical simulations and experiments. *Int J Multiph Flow* 56:81–92
- Foissac A, Malet J, Mimouni S, Feuillebois F (2010) Binary water droplet collision study in presence of solid aerosols in air. In: *Proceedings 7th international conference on multiphase flow, ICMF2010, Tampa, FL USA, May 30–June 4 2010*
- Fritsching U, Gao S (2010) Droplet-particle collisions in intersecting melt sprays. *At Sprays* 20:31–40
- Gao T-C, Chen R-H, Pu J-Y, Liu T-H (2005) Collision between an ethanol drop and a water drop. *Exp Fluids* 38:731–738
- Gavaises TL, Theodorakakos A, Bergerles G, Brenn G (1996) Evaluation of the effect of droplet collisions on spray mixing. *Proc Inst Mech Eng* 210:465
- Gotaas C, Havelka P, Jakobson HA, Svendsen HF (2007a) Evaluation of the impact parameter in droplet collision experiments by the aliasing method. *Phys Fluids* 19:102105
- Gotaas C, Havelka P, Jakobson HA, Svendsen HF, Hase M, Roth N, Weigand B (2007b) Effect of viscosity on droplet collision outcome: experimental study and numerical comparison. *Phys Fluids* 19:102106
- Guo B, Fletcher DF, Langrish TAG (2004) Simulation of the agglomeration in a spray using Lagrangian particle tracking. *Appl Math Model* 28:273–290
- Ho CA, Sommerfeld M (2002) Modelling of micro-particle agglomeration in turbulent flow. *Chem Eng Sci* 57:3073–3084
- Hou S, Schmidt T (2006) Adaptive collision meshing and satellite droplet formation in spray simulations. *Int J Multiph Flow* 32:935–956
- Jiang YJ, Umemura A, Law CK (1992) An experimental investigation on the collision behavior of hydrocarbon droplets. *J Fluid Mech* 234:171–190
- Ko GH, Ryou HS (2005a) Modeling of droplet collision-induced breakup process. *Int J Multiph Flow* 31:723–738
- Ko GH, Ryou HS (2005b) Droplet collision process in an inter-spray impingement system. *Aerosol Sci* 36:1300–1321
- Kollar L, Farzaneh M, Karev AR (2005) Modeling droplet collisions and coalescence in an icing wind tunnel and the influence of these processes on droplet size distribution. *Int J Multiph Flow* 31:69–92
- Kuschel M, Sommerfeld M (2013) Investigation of droplet collisions for solutions with different solids content. *Exp Fluids* 54:1440
- Matsuo S, Makita T (1989) Viscosities of six 1-alkanols at temperatures in the range 298–348 K and pressures up to 200 MPa. *Int J Thermophys* 10:833–843
- Munnannur A, Reitz RD (2007) A new predictive model for fragmenting and non-fragmenting binary droplet collisions. *Int J Multiph Flow* 33:873–896

- Naue G, Bärwolff G (1992) *Transportprozesse in Fluiden*. Deutscher Verlag für Grundstoffindustrie GmbH, Leipzig
- Nijdam JJ, Guo B, Fletcher DF, Langrish TAG (2006) Lagrangian and Eulerian models for simulating turbulent dispersion and coalescence of droplets within a spray. *Appl Math Model* 30:1196–1211
- Pineiro MM, Garcia J, de Cominges BE, Vijande J, Valencia JL, Legido JL (2006) Density and surface tension variation with temperature for n-nonane and 1-hexanol. *Fluid Phase Equilib* 245:32–36
- Planchette C, Lorenceau E, Brenn G (2012) The onset of fragmentation in binary liquid drop collisions. *J Fluid Mech* 702:5–25
- Post SL, Abraham J (2002) Modeling the outcome of drop–drop collisions in Diesel sprays. *Int J Multiph Flow* 28:997–1019
- Qian J, Law CK (1997) Regimes of coalescence and separation in droplet collision. *J Fluid Mech* 331:59–80
- Rabe C, Malet J, Feuillebois F (2010) Experimental investigation of water droplet binary collisions and description of outcomes with a symmetric Weber number. *Phys Fluids* 22:047101
- Rüger M, Hohmann S, Sommerfeld M, Kohnen G (2000) Euler/Lagrange calculations of turbulent sprays: the effect of droplet collisions and coalescence. *At Sprays* 10:47–81
- Shannon C (1948) A mathematical theory of communication. *Bell Syst Tech J* 27, 379–423 and 623–656
- Sommerfeld M (2001) Validation of a stochastic Lagrangian modelling approach for inter-particle collisions in homogeneous isotropic turbulence. *Int J Multiph Flows* 27:1828–1858
- Sommerfeld M, Kuschel M (keynote lecture) (2013) Collisions of high viscous droplets: experiments and modelling. In: CD-ROM Proceedings 8th international conference on multiphase flow, ICMF2013, Jeju, Korea, May 26–May 31 2013, Paper No. 849
- Tsuru D, Tajima H, Ishibashi R, Kawauchi S (2010) Droplet collision modelling between merging immiscible sprays in direct water injection systems. In: ILASS-Europe 2010, 23rd annual conference on liquid atomization and spray systems, Brno, Czech Republic, September 2010
- Willis K, Orme M (2003) Binary droplet collisions in a vacuum environment: an experimental investigation of the role of viscosity. *Exp Fluids* 34:28–41